Y CURRENT AND STAGNATION ZONE ALYSIS IN ECD DURING OUTWARD MODE OF ELECTROLYTE FLOW

by

YASHAVANT KANETKAR

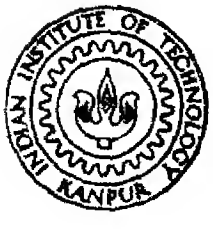

DEPARTMENT OF MECHANICAL ENGINEERING

AN INSTITUTE OF TECHNOLOGY, KANPUR

JULY, 1987

STRAY CURRENT IN ... ANALYSIS IN ECD DURING OUTWARD MODE OF ELECTROLYTE FLOW

A Thesis Submitted
In Partial Fulfilment of the Requirements
for the Degree of

MASTER OF TECHNOLOGY

by

YASHAVANT KANETKAR

to the

DEPARTMENT OF MECHANICAL ENGINEERING

INDIAN INSTITUTE OF TECHNOLOGY, KANPUR

JULY, 1987

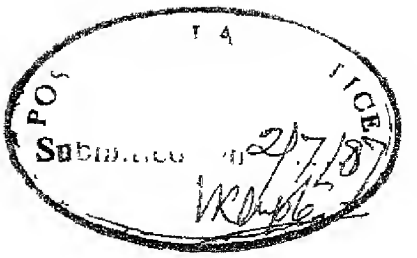

CERTIFICATE

Certified that this thesis work entitled, "STRAY CURRENT AND STAGNATION ZONE ANALYSIS IN ECD DURING OUTWARD MODE OF ELECTROLYTE FLOW" submitted by Shri Yashavant Kanetkar in partial fulfilment of the requirements for the degree of MASTER OF TECHNOLOGY of the Indian Institute of Technology, Kanpur is a record of bonafide research work carried out by him under our guidance and supervision. The work embodied in this thesis has not been submitted elsewhere for a degree.

(G.K. Lal)
Professor
Department of Mechanical Engg.
Indian Institute of Technology
Kanpur

(V.K. Jain)
Assistant Professor
Department of Mechanical Engg.
Indian Institute of Technology
Kanpur

ACKNOWLEDGEMENTS

Working on a thesis is a task that cannot be done by an individual in isolation. I have been no exception to this rule and have gratefully accepted the helping hand offered by many. Those whom I would like to specially mention are-

- First and foremost, Dr. V.K. Jain for his inspiring guidance, meticulous attention, constructive criticism and above all for his untiring devotion throughout the tenure of this work.
- Dr. G.K. Lal for his invaluable advice and suggestions.
- Dr. T. Sundararajan for his useful suggestions during different stages of this work.
- Thanks are due to all my friends at IIT-Kanpur of whom Chitta and Tandon deserve a special mention.

-YASHAVANT KANETKAR

CONTENTS

LIST OF TABLES

LIST OF FIGURES

NOMENCLATURE

A	Atomic weight of the work material
A_r	Area (cm^2)
C_e	Specific heat of electrolyte (erg/gm°C)
D	Hydraulic mean diameter (cm)
E	Electrochemical equivalent (gm/Coulomb)
f	Feed rate (cm/sec)
f_n	Feed rate vector normal to the work surface (cm/sec)
F	Faraday's constant (Coulomb)
I	Current (ampere)
J	Current density (ampere/cm^2)
K	Electrolyte conductivity (Ohm^{-1} cm^{-1})
K_s	Conductivity at the end of stagnation zone (Ohm^{-1} cm^{-1})
KIN	An index used to count the number of computational cycles
N_i	Interpolating function/shape function
$N_{,x}$, $N_{,y}$	Derivatives of interpolating functions
n	Void fraction exponent (constant)
P	Electrolyte pressure in the IEG (gm/cm^2)
$\dot{Q}$	Discharge of electrolyte (cm^3/sec)
R_e	Electrical resistance (Ohm)
R_n	Reynold's number
r, r', R	Radius (cm)
r_1	Inner radius of tool (cm)

r_2	Outer radius of tool (cm)
r_{tc}	Tool corner radius (cm)
R_{a1}	Work corner radius (cm)
t	Time (sec)
T	Temperature (°C)
T_s	Temperature at the end of stagnation zone (°C)
T_{sz}	Temperature at the end of side zone (°C)
U	Electrolyte flow velocity (cm/sec)
V	Applied voltage (volt)
X, x	Distance along electrolyte flow direction (X coordinate) (cm)
Y, y	Coordinate measured in Y direction (cm)
Z	Valency of electrochemical dissolution
α	Temperature coefficient of electrical conductivity of electrolyte ($°C^{-1}$)
α_v	Void fraction
Δe	Area of an element (cm^2)
Δt	Computational cycle time (sec)
ΔT	Incremental change in temperature (°C)
ΔV	Overpotential (volt)
η	Current efficiency or machining efficiency
Θ	Angle between the direction of feed and normal to the work surface (degrees)
ρ	Mass density (gm/cm^3)
σ	Gas slip ratio
μ	Viscosity of the electrolyte (dyne sec/cm^2)
ϕ	Electric field potential (volt)

SUBSCRIPTS

a	Anode
e	Electrolyte, element
g	Gas
i,j	Node number
o	Initial condition
tc	Tool corner
w	Work material

SUPERSCRIPTS

e	Element
ne	Nodes of an element

ACRONYMS

BEM	Boundary element method
ECD	Electrochemical drilling
FDT	Finite difference technique
FEM	Finite element method
IEG	Interelectrode gap
MRR	Metal removal rate
OWS	Obtained work shape
RWS	Required work shape

SYMBOLS

[ ]	Row matrix
{ }	Column matrix
[ ]	Square matrix

ABSTRACT

The Electrochemical Machining (ECM) is one of the most widely used unconventional machining process. However, the potential of this highly capable process has not been fully exploited due to the inherent complexities of the process, like, simultaneous occurrence of two phase fluid dynamics, unsteady state heat transfer, mass transfer, thermodynamics, electrostatics and electrochemistry between moving boundaries. This complicates the problem of anode shape prediction in ECM many folds. Majority of the models available for anode shape prediction are based on simplified assumptions.

In the present work, a modified anode shape prediction model has been proposed which predicts the anode profile in stagnation, front, transition, side and stray current zones. This model accounts for the variation in different process parameters during machining. Experimental data has been used to ascertain the accuracy of the model. Comparison of analytically predicted and experimentally obtained anode profile reveals a reasonable agreement between the two. The effects of the assumptions made and the experimental errors and their possible contribution in causing the deviations between theory and experiments have been discussed.

Conventional ECM tool design is not accurate enough to account for different complex phenomenon taking place in the domain of interest. A method has been suggested for determination of the shape of the tool (cathode) (specifically accounting for the effects of stray current zone) to produce the required work (anode) shape, while machining under specified conditions. The tool design model has been further extended to predict the tool shape which will produce a spike of specified size in the stagnation zone. This model can be used for analysing the problems of tool design for external shaping by ECM. This method accounts for variation in different process parameters. The cathode shape prediction problem has been attempted for electrochemical drilling with a bare tool. Tools have been designed for producing profiles obtained experimentally. Tool design has also been carried out for straight sided holes with the top surface flat, as well as for a reasonably small spike in the stagnation zone. Comparison of designed and experimental tool shapes reveal good agreement.

CHAPTER I

INTRODUCTION AND LITERATURE SURVEY

1.1 ELECTROCHEMICAL MACHINING (ECM)

Advanced technological developments in industries like aerospace, nuclear etc. have been accompanied by development of materials which are exceedingly difficult to machine. These materials have been developed to meet the demand of high strengt and heat resistance. These rapid developments in the field of materials have given an impetus to the manufacturing technology to develop, modify and discover newer technological processes with a view to achieve results that are far beyond the scope of existing conventional manufacturing processes. This has led to the development of new techniques of machining such as ECM, EDM USM, AJM, EBM etc. These unconventional processes are capable providing effective solutions to the problems imposed by the increasing demand for accurate machining of high-strength-temperature-resistant (HSTR) alloys, the requirements of parts with complex geometries, and materials so hard as to defy machi ing by conventional methods.

Of all the unconventional machining processes, Electrochemical machining is the one that is most widely used. ECM is a process of metal removal from an electrically conducti workpiece by controlled and accelerated anodic dissolution. High velocity electrolyte flows between anode and cathode

(Figure 1.1) subjected to a small d.c. voltage and a small interelectrode gap (IEG) is maintained between them. The flowing electrolyte helps not only in allowing the high rate of metal dissolution, but also carries away the reaction products and heat generated during the electrochemical reaction.

The advantages of ECM process lie in its ability to machine very hard metals without causing any tool wear, high metal removal rate, no structural damage to the workpiece and capability to machine complicated shapes with good surface finish. The various areas of application [1] of ECM are drilling, boring, turning, cavity sinking, milling, grinding etc. Although, the applications of ECM are many, its capabilities have not been fully exploited due to lack of clear understanding of complex nature of the process of metal removal and non-existence of an efficient tool design methodology.

The metal removal rate (MRR) in ECM depends upon a large number of interrelated parameters. Most of the machining parameters such as electric field distribution, electrolyte conductivity (K), temperature rise (ΔT), valency of dissolution (Z), electrolyte flow velocity (U), etc. are varying simultaneously and continuously along the electrolyte flow path with machining time. Further, the interaction of these parameters is of complex nature which makes it further difficult to understand the exact mechanism of metal removal. Moreover, the electrolyte in the IEG is a mixture of liquid electrolyte, gases evolved

during electrochemical reaction and precipitates. In majority of cases, it is difficult to evaluate the flow parameters due to the effects of electrolyte starvation and cavitation. Thus, ECM is a fairly complicated phenomenon since it involves simultaneous occurrence of two-phase fluid dynamics, heat transfer, mass transfer, thermodynamics and electrochemistry between moving boundaries.

Further, the accuracy of machining is governed by how accurately the tools can be designed, which in turn depends upon the accuracy of anode shape prediction model. With this in view different models available in literature for cathode and anode shape prediction have been discussed below.

1.2 TOOL DESIGN FOR ECM

The tooling problem is of great concern because it is usually linked with high cost. A direct method for deciding upon the tool shape is almost impossible for all but the simplest of work shapes. In practice, a 'trial and error' method usually has to be relied upon, with repetitive machining runs having to be made to obtain the correct tool geometry.

The designing of tools for ECM can be classified under two heads. First is the determination of shape of tool together with optimum machining conditions necessary to produce the required work shape [2]. The second aspect is a practical one, which is concerned with making the tool

of an appropriate material, fixing it in the machine, connecting it to the power supply and passing an adequate supply of electrolyte between tool and workpiece. The design requirements for some of these aspects might turn out to be conflicting and therefore may call for certain modifications in the tool geometry. Here, only part of the first aspect of tool design has been considered, i.e., designing the tool shape for producing desired work profile ECM deals with computation of tool shape which under specif machining conditions would produce a work having a prescrib shape or profile. Inversely, the problem of anode shape prediction deals with determining the work shape obtainable from a tool of known geometry when machining is performed under specified machining conditions [4,5]. The workpiece profile is usually computed from the equilibrium gap. The IEG is not uniform in ECM and it is influenced by a number of parameters such as electrolyte flow rate, work material microstructure, change in valency of dissolution of the work-material during machining, type of electrolyte, curren density, stray current attack etc. The influence of all these continuously varying parameters is not well known, which makes the anode shape prediction difficult.

In general, the practical methods like 'trial and error' methods for obtaining the tool shape are expensive, time consuming and inaccurate. Several attempts have been

made to develop a comprehensive model of the mechanics of metal removal in ECM. Some of the models for anode shape prediction and cathode shape design are discussed below.

1.3 COSθ METHOD

This method was first proposed by Tipton [6,7] for the computation of equilibrium gap for any given operating conditions. This method excludes the considerations of the mode of electrolyte flow, overpotential, variation in electrolyte conductivity, heat transferred to the electrodes etc. This method can be applied to the electrode regions where the electric field can be assumed to be normal to the electrode surfaces. In this method equilibrium workshape is computed corresponding to the tool whose profile has to be approximated by several planar sections inclined at different angles, say, θ as shown in Figure (1.2).

For plane parallel electrodes with their surfaces normal to the direction of feed, the equilibrium gap, Y_e, is given by

$$Y_e = \frac{K (V - \Delta V)}{F \rho_w f} \qquad (1.1)$$

where, K is the electrolyte conductivity, (V- V) is the effective voltage, F is the Faraday's constant, ρ_w is the mass density of the work and f is the feed rate of the tool.

The equilibrium gap between any section of cathode surface and the corresponding surface of the anode which is parallel to it is given by, $Y_e/\text{Cos}\Theta$. The angle 'Θ' is measured between normal to the anode surface and the direction of the cathode feed. The cathode shape for a given anode surface can be computed from the following equations.

Let $Y = f(x)$ represent the anode surface. Then any point, say $A(x, y)$, on the anode surface has a corresponding point, say $B(x_1, y_1)$ on the cathode surface. The gap width between A and B then becomes $Y_e/\text{Cos}\Theta$ (Figure 1.2). We have,

$$Y - Y_1 = AB\ \text{Cos}\Theta = Y_e \qquad (1.3)$$

and

$$X_1 - X = AB\ \text{Sin}\Theta = Y_e\ \tan\Theta,$$

or

$$X_1 - X = Y_e \left(\frac{dY}{dX}\right) . \qquad (1.4)$$

By substituting the values of X and Y from equations (1.3) and (1.4) in equation (1.2) gives the equation for the cathode surface.

The '$\text{Cos}\Theta$' method is generally applicable to the regions where the local radii of curvature of the anode and cathode surfaces are large compared with the equilibrium gap. This method excludes the effect of different process

parameters on predicted anode profile. Workpieces having sharp corners and complex shapes cannot be analysed with this method.

1.4 NOMOGRAPHIC APPROACH

König [4] and Ganesh [8] suggested the nomographic approach to evaluate the equilibrium anode shape. König [4] has prepared a nomogram for calculating the side gap for known values of equilibrium gap, tool radius and bare tool length. Ganesh [8] has developed separate nomograms for evaluating the equilibrium gap and tool feed rate. Tool feed rate is calculated for the given current and area of cross-section of the tool. The equilibrium gap is then evaluated from the thus calculated feed rate and the given voltage. Nomograms facilitate planning of ECM operations, but since they have been prepared with many simplified assumptions they have not gained much popularity. Moreover, they are applicable for specific machining conditions and work-tool combinations.

1.5 CONTINUITY METHOD

Lawrence [9] developed a graphical technique for tool design by solving the field equation in the gap. But this procedure gives low accuracy and is tedious. He subsequently adopted numerical methods to solve the field equation using digital computer. In this method, starting from

a defined equipotential work shape boundary, a model of electric field is constructed, where each new equipotential surface is a possible tool shape which will produce the original work shape. This method rests on the assumption that Ohm's law applies across a small element of electrolyte and that the current flowing between a pair of flux lines in an electric field is constant. It does not take into account the variation in electrolyte properties in the IEG along the flow path.

1.6 CATHODE SHAPE PREDICTION BY DRAWING CURVILINEAR SQUARES IN THE IEG

Tipton [10] has developed a method for determining the tool shape by drawing curvilinear squares between the work and tool boundaries. The work surface is defined numerically in XY plane. Y is taken as feed direction and coordinates are spaced by constant X increment equal to a fraction of the equilibrium gap. The work boundary is considered as equipotential with each coordinate representing the end of a current flow line. In equilibrium, the normal current density being constant, a constant current increment ΔI flows between each of the adjacent coordinates on the work boundary since they are equally spaced in X-direction. By using each adjacent pair of coordinates, it is possible to draw the curvilinear squares and to construct the first row of potential field distribution between work and tool as shown in Figure 1.3. If the X coordinate spacing is Y_e/n, then

applying the above process repetitively will result in n^{th} equipotential which is also the tool surface. Each intermediate surface is also a possible tool surface for equilibrium gaps as Y_e/n, $2Y_e/n$, $3Y_e/n$, $4Y_e/n$, etc.

This method is error prone, especially when the process is repeated several times, since it is based on differentiating the input data for drawing curvilinear squares, and when repeated any random error in the input data gets magnified. Complete failure of calculation occurs when two current flow lines cross each other. In such a case, the previous equipotential could be used as a tool with the fractional equilibrium gap associated with it. This model does not account for variations in the process parameters.

1.7 NUMERICAL METHODS

The emergence of fast digital computers has led to the application of numerical techniques to simulate the ECM process. In ECM, during machining, local current density causes the change in the shape of workpiece. Further, the current density in turn changes with the changing work-shape. To determine the current density, it is necessary to solve Laplace equation for the field distribution in the IEG. The three popular methods used to determine the potential distribution are discussed below.

1.7.1 FINITE DIFFERENCE TECHNIQUE (FDT)

Tipton [6] and, Hopenfeld and Cole [11] applied FDT to determine potential distribution in the IEG, assuming constant conductivity and temperature.

Figure (1.4) shows the tool work surfaces drawn in square meshes containing a set of grid points of general coordinates (i, j). The grid points on the cathode boundary are assigned zero potential values, and those on the anode boundary are set to some known values. The initial potential at the grid points within the IEG region are set by linear interpolation along the vertical grid lines between anode and cathode. These values must be progressively adjusted until they satisfy a finite difference equation corresponding to Laplace's equation in the region between the boundaries.

For a point 'O' located in a mesh of spacing h(i,j), the finite difference equation corresponding to Laplace's equation becomes,

$$\frac{\partial^2 \phi}{\partial x^2} + \frac{\partial^2 \phi}{\partial y^2} = 0 \qquad (1.5)$$

Using equation (1.5), the potential at 'O' can be obtained as,

$$\phi(i,j) = \frac{(\phi_{i+1,J} + \phi_{i-1,J} + \phi_{i,j+1} + \phi_{i,j-1})}{4} \qquad (1.6)$$

In some cases, all points on the anode and cathode boundary may not lie on the grid points. In such cases, it is customary to relax the potential by linear interpolation. Nanayakkara and Larsson [12] have suggested the use of irregular grids along with regular grids to account for complex geometries.

1.7.2 FINITE ELEMENT METHOD (FEM)

In majority of cases, the IEG is complex shaped. As a result, the cathode and anode boundaries cannot be matched accurately using square meshes, which introduces further approximations. In order to overcome this problem, Jain and Pandey [13] suggested the application of FEM to analyse the complex shaped IEG.

Jain [3] has developed FEM models, FET-11 and FET-22, for the prediction of anode profiles in case of plane parallel machining. The model FET-11 is based on use of Ohm's law for the calculation of current densities in the IEG, and FEM has been applied for one dimensional problem to obtain temperature distribution within the IEG. In the model FET-22, Laplace equation has been solved to obtain potential distribution within the IEG from which current densities are calculated. Jain also extended model FET-11 (and named it as SGFET-11) for predicting the anode profile in case of rectangular and cylindrical deep hole drilling operations. All these models are capable to predict the anode shape accurately, by taking

into consideration, the variations in different process parameters. Murugan [14] and Yogindra [15] have extended FEM models for anode shape prediction using bit type of tools. Ravi Raju [16] has modified model SGFET-22 for cathode design of bare and bare bit tools. In all these models however, the stray current zone and the stagnation zone have been neglected.

1.7.3 BOUNDARY ELEMENT METHOD (BEM)

Both the methods, FDM and FEM are domain based requiring frequent grid regeneration to compensate for the movement of work boundary during simulated ECM. Also, both FDM and FEM yield solutions corresponding to internal as well as boundary nodes, but in most of the cases, internal solutions are unnecessary when predicting the workpiece boundary and designing the cathode shape. In BEM unlike FDM and FEM, boundary alone is discretized into segments. This considerably reduces the amount of input data and its preparation time. However, if required the solution to internal points can also be obtained.

Narayanan, Hinduja and Noble [17] have applied BEM, for the anode shape prediction in ECM. Linear and quadratic elements were used to represent the boundaries. It was concluded that with far less computational effort, a comparatively better accuracy is obtained using BEM. However for a clear understanding of the process solutions at internal nodes are also required.

1.8 ANODE SHAPE PREDICTION IN STRAY CURRENT ZONE AND STAGNATION ZONE

1.8.1 STRAY CURRENT ZONE

The distribution of electric flux lines during ECD is such that some portion of the workpiece which is far away from the tool also undergoes dissolution, due to current lines acting over this zone (Figure 1.5). This effect is called as stray current effect and the zone over which the stray current acts is called as stray current zone. Stray current attack is undesirable not just because of poor dimensional accuracy but also because etched and pitted surfa are obtained in this zone, as reported by Hoar and Mears [18 Rather than predicting the anode shape in stray current zone for a particular type of electrolyte, the trend in literature was observed to be of minimizing the stray current attack by choosing an appropriate electrolyte or by modifying the properties of a given electrolyte. Boden and Evans [19] showed that the effect of stray current attack could be reduced to a certain extent by bringing about passivation in the stray current zone by addition of small amount of another suitable salt to the electrolyte. They suggested that the additive could be carbonate in the case of machinin of Iron and Nickle, which would form a sparingly soluble reaction product with the workpiece and hence bring about passivation by precipitation of insoluble products in the pi of stray current zone. $NaClO_3$ was found suitable for machir

of cobalt. LaBoda and Mcmillan [20] has suggested the use of sodium chlorate as electrolyte for machining of any steel workpiece including high alloy steels because of its low 'throwing power' which ensures that the cutting is concentrated in areas close to the cathode, as is desired.

Bannard [21] has pointed out that the extent of stray current could be controlled to a certain extent by use of a "thief-anode" (Figure 1.6) which steals away the current flux which is not normal to the tool face. The disadvantage of this method is the difficulty in the manufacturing of the tool.

1.8.2 STAGNATION ZONE

Little literature appears to be available till date, discussing about the profile of the spike that is formed in ECD of blind holes. Larsson and Muzaffaruddin [22] assumed radial current density distribution to determine the spike height. The purpose of their analysis was to show how the shaping performance of electrolytes is related to their electrochemical properties. They used the spike heigh as an index to demonstrate the effect of solution properties on its shaping performance rather than to predict the actual spike profile. The use of a simple tubular drill with an uninsulated bore constituted a very sensitive test for shapi performance, as the height of the spike produced at the bott

of a blind hole is shown to be dependent on both polarisation and current efficiency. They showed that the development of a current density dependent voltage at the electrode-electrolyte interface, and efficiency of an electrolyte are far from negligible in determining the shaping performance of an electrolyte. This is particularly so when machining is in generating mode where there is a wide range of current density. They concluded that polarization plays an important role in reducing the shaping performance of an electrolyte and should not be ignored in any method used to predict work-shapes. Here, the assumptions made are far reaching, since the current distribution at the top of the spike will certainly not be radial. Also, the change in electrolyte conductivity due to heating effects and the development of gas bubbles in the electrolyte has not been taken into account

1.9 PRESENT WORK

From the above literature survey, it appears that no attempt has been made to determine the effect of stray current attack on predicted anode shape. Also, no analysis appears to be available to find out the profile of the spike that is formed in the stagnation zone during electrochemical drilling of blind holes. For a comprehensive and meaningful analysis o anode shape prediction during ECD, the analysis of stray curre zone and stagnation zone is very important. The work embodied

in the first part of this thesis has been aimed towards the development of anode shape prediction model to analyse the effect of stray current attack on the anode profile. The anode shape prediction model (SGFET-22) developed by Yogindra [15] has been modified by incorporating the stray current zone. The model has been named as STZFET-22. This model has been extended to determine analytically, the profile of spike generated in stagnation zone during ECD. The analytical anode profile obtained by STZFET-22 has been compare with experimental profile obtained by Jain [3] .

The second part of the work has been aimed towards the development of a computer aided method for the tool design for ECM. The two dimensional cathode (tool) shape prediction model for ECD proposed by Ravi Raju [16] has been modified to account for stray current zone and stagnation zone. The anode shape prediction model STZFET-22 has been used in this design package for electrochemical drilling. Tools have been designe for producing the specified work shapes, while machining under prescribed machining conditions. Designed tool shapes have been compared with experimental tool shapes used by Jain [3] for electrochemical drilling. Design of electrolyte supply hole in the cathode has been aimed to minimize the spik dimensions, especially the height. This is a case similar to the tool design for external shaping by ECM process. The tool design model has been named as STZDES-22.

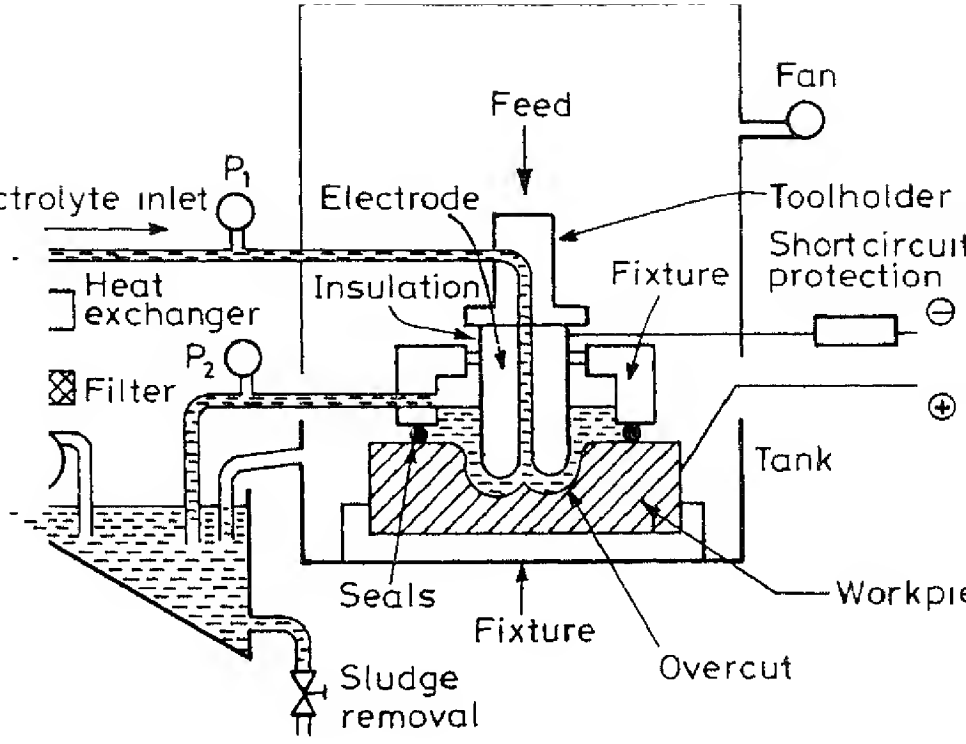

.1 BASIC SCHEME OF ELECTRO-CHEMICAL
NING PROCESS.

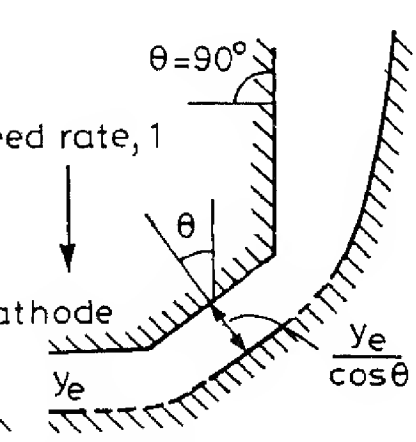

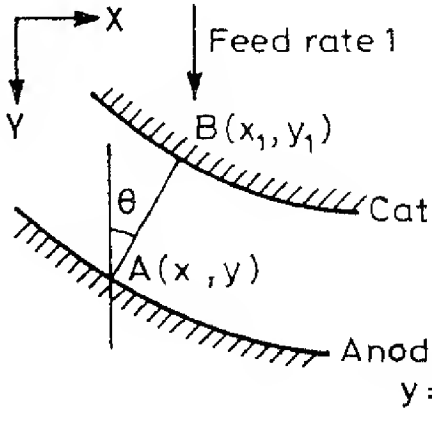

rinciple of the cos θ method (b) Cathode design by c

FIG. 1.2 Cos θ METHOD

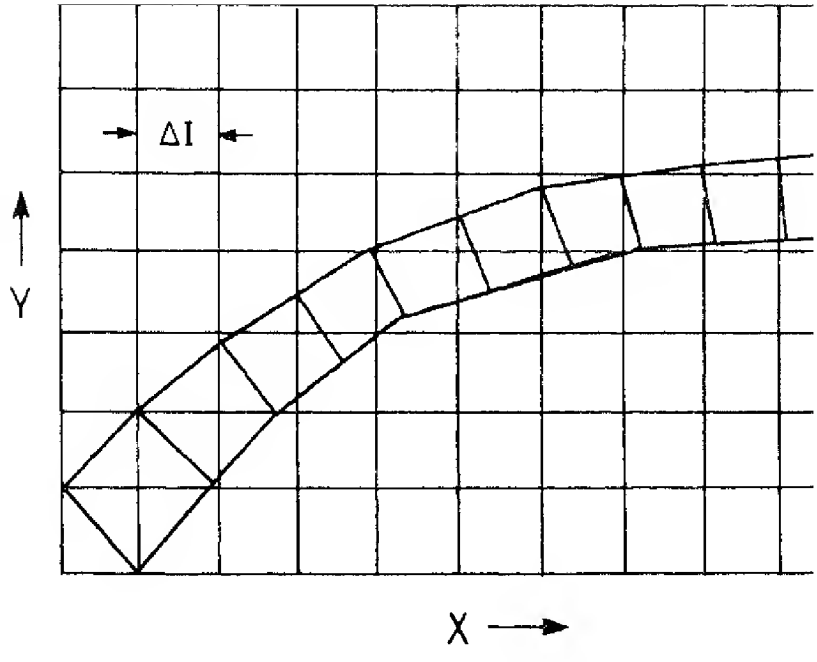

The first step in calculating a tool sh
culating the field distribution betwee
tool as a series of curvilinear squa

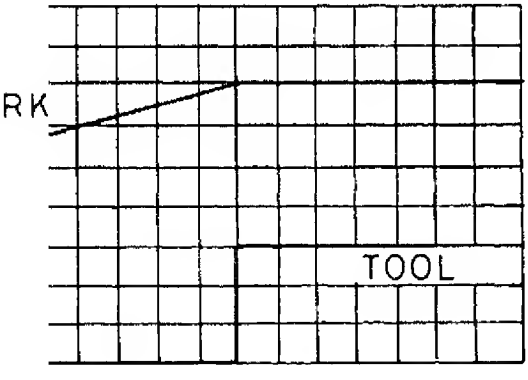

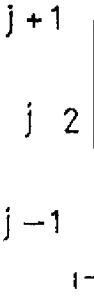

tool work system discretized
uare meshes

(b) A squre
h with

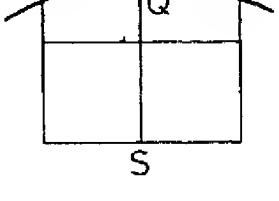

(c) Boundary forms irregular star with one

F'g 1 4 Finite d'fference technique

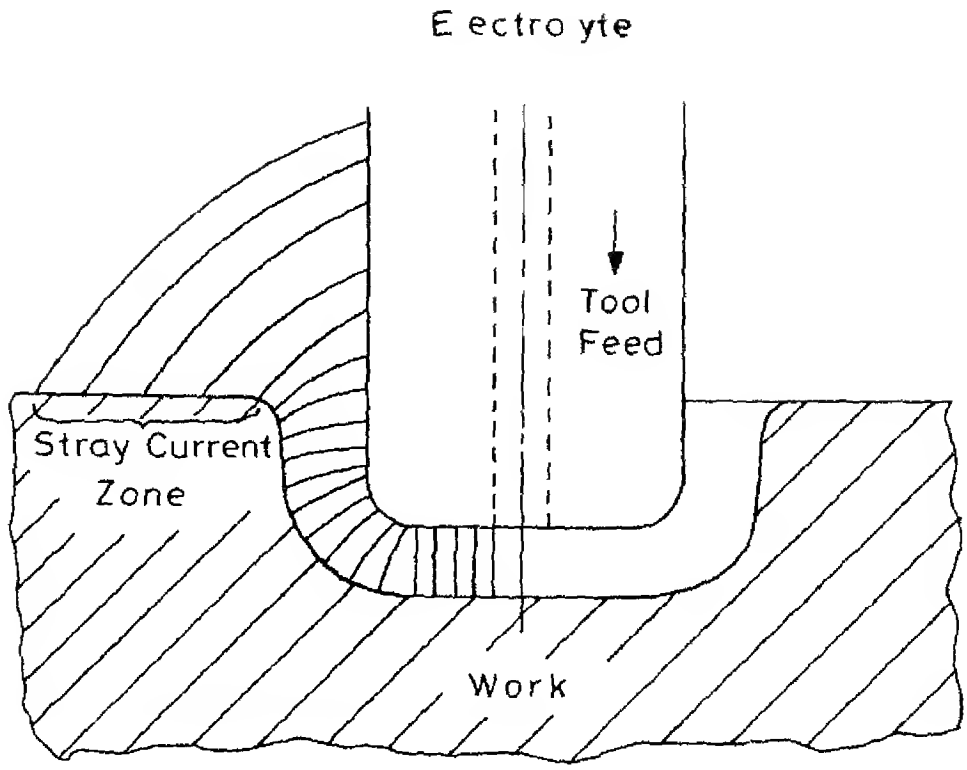

Fig. 1.5 Distribution of electric flux lines in

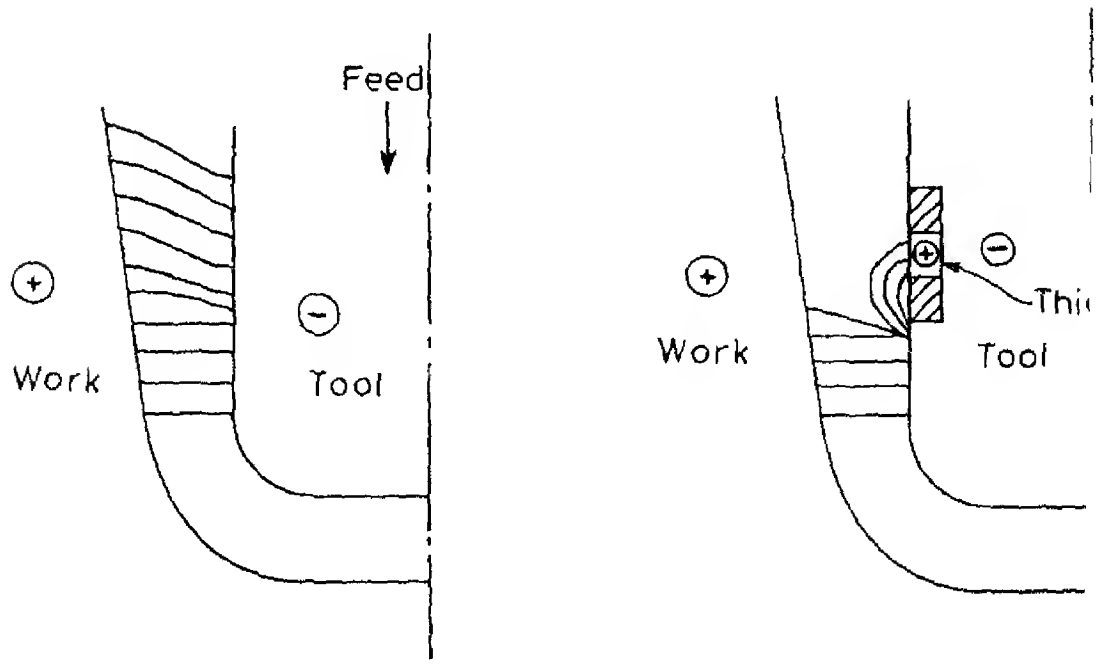

(a) Current lines for normal tooling

(b) Current lines usin anode

Fig. 1.6 Principle of Thief Anode [21]

CHAPTER II

THEORETICAL ANALYSIS

2.1 INTRODUCTION

The ability to predict the variations in process parameters for any given operating conditions is a pre-requisite for proper design of tools in ECM. In this chapter, the expressions for various process parameters such as electrolyte flow velocity, electrolyte conductivity current density, temperature distribution etc. have been derived for electrochemical drilling. In the present work, ECD with outward mode of electrolyte flow has been analysed. However, the same analysis can be applied for the case of inward mode of electrolyte flow with small changes in the computational scheme. To make a comprehensive analysis, all the five zones (Figure 2.1) namely, stagnation, front, transition, side and stray current have been analysed individually with suitable assumptions mentioned therein. The stagnation zone has been divided into three zones as shown in Figure (2.1). The three zones are named as stagnation transition (S.T. zone), stagnation side zone (S.S. zone) and stagnation stray current zone (S.S.C. zone).

2.2 ANALYSIS OF ELECTROCHEMICAL DRILLING

2.2.1 ELECTROLYTE FLOW VELOCITY (U)

In the present work, the mode of electrolyte flow is outward and separate expressions have to be derived for stagnation, front, transition, side and stray current zones. The assumptions made for calculation of electrolyte flow velocity are:

(i) Electrolyte is an ideal fluid.

(ii) The volume of electrolyte flowing at any section per unit time is constant.

(iii) Cavitation and starvation of the electrolyte are neglected.

(iv) Electrolyte velocity across the flow direction is assumed to be uniform

2.2.1.1 STAGNATION ZONE

As the inner tool corner radius is very small electrolyte flow in S.T. zone, S.S. zone and S.S.C. zone (Figure 2.1) can be considered to be in axial direction. The following analysis to determine electrolyte flow velocity holds good in all the three zones, i.e. S.T. zone, S.S. zone and S.S.C. zone. Referring to Figure (2.2),

$$A_r = (\pi r_1^2 - \pi(r_1 - y)^2)$$

or,

$$A_r = \pi(2r_1 y - y^2) \qquad (2.1)$$

and

$$U = \frac{\dot{Q}}{\pi(2r_1\ y - y^2)} \qquad (2.2)$$

where, $\dot{Q}$ is discharge of electrolyte/unit time.

2.2.1.2 FRONT ZONE

In this zone, the electrolyte flow is assumed to be in radial direction. Electrolyte flow velocity at any radius (Figure 2.3a) from the axis of the tool is given by,

$$U = \frac{\dot{Q}}{A_r} = \frac{\dot{Q}}{2\pi r\ Y} \qquad (2.3)$$

2.2.1.3 TRANSITION AND SIDE ZONES

For calculation of electrolyte flow velocity in transition zone, following assumption has been made. If the X coordinate of the node at which flow velocity is being calculated is less than the outer radius of the tool (r_2) then that particular node is considered to be in front zone, otherwise it is considered to be in side zone. In side zone, the electrolyte flow is assumed to be in axial direction.

From Figure (2.3c),

$$A_r = \pi(r_2 + Y)^2 - r_2^2$$

or

$$A_r = \pi(Y^2 + 2r_2\ Y)$$

and

$$U = \frac{\dot{Q}}{\pi(Y^2 + 2r_2Y)} \qquad (2.4)$$

2.2.1.4 STRAY CURRENT ZONE

For finding out the velocity of electrolyte, Laplace equation has been solved for velocity potential. Here, the following assumption has been made. In stray current zone at edge AD (Figure 2.4), velocity is perpendicular to AD, which means $\nabla\phi = 0$, i.e. ϕ = constant along edge AD. For convenience, ϕ has been taken to be equal to zero along edge AD.

For a two dimensional case the Laplace equation can be written as,

$$\frac{\partial^2\phi}{\partial x^2} + \frac{\partial^2\phi}{\partial y^2} = 0 .$$

Using simple triangular elements (Figure 2.4), the velocity potential (ϕ) has been assumed to vary linearly within the element throughout the solution domain. This velocity potential (ϕ) can be represented by a polynomial

$$\phi^e = a + bx + cy . \qquad (2.5)$$

The equation (2.5) can also be written in terms of the interpolating functions, N_i, at each node,

$$\text{i.e.} \quad \phi^e = N_1\phi_1 + N_2\phi_2 + N_3\phi_3 = [N]^{(e)} \{\phi\}^{ne} \tag{2.6}$$

Substituting equation (2.6) in equation (2.5), the residue becomes

$$R^e = \frac{\partial^2 \phi^e}{\partial x^2} + \frac{\partial^2 \phi^e}{\partial y^2} .$$

By Galerkin's method,

$$\iint N_i R^e \, dx \, dy = 0, \quad i = 1,2,3$$

i.e.

$$\iint N_i \left(\frac{\partial^2 \phi^e}{\partial x^2} + \frac{\partial^2 \phi^e}{\partial y^2}\right) dx \, dy = 0 .$$

Integrating by parts w.r.t. x for the first term and w.r.t. y for the second term, gives

$$\left(\frac{\partial N_i}{x} \frac{\partial \phi^e}{x} + \frac{\partial N_i}{y} \frac{\partial \phi^e}{y}\right) dx \, dy =$$

$$\oint N_{iB} \left(\frac{\partial \phi^e}{\partial x} n_x + \frac{\partial \phi^e}{\partial y} n_y\right) \tag{2.7}$$

where, n_x and n_y are the direction cosines along X and Y axis respectively, on the boundary of the domain.

Using equation (2.6) and writing the equation (2.7) in matrix form gives

$$\int \left(\frac{\partial N_i}{\partial x}\left[\frac{\partial N}{\partial x}\right] + \frac{\partial N_i}{\partial y}\left[\frac{\partial N}{\partial y}\right]\right)\{\phi\}^{ne}\, dx\, dy = \oint N_{iB}\, V_n\, dB$$

', V_n is the normal velocity,

$$[K]^{(e)}\ \{\phi\}^{(ne)} = \{V_n\}^{(e)} \qquad (2.8)$$

',

$$K^{(e)} = \int\int \left(\frac{\partial N_i}{\partial x}\left[\frac{\partial N}{\partial x}\right] + \frac{\partial N_i}{\partial y}\left[\frac{\partial N}{\partial y}\right]\right) dx\, dy$$

$$\{V_n\}^{(e)} = \oint N_{iB}\ V_n \quad dB.$$

For an element, the matrix form of finite element tion becomes,

$$\begin{bmatrix} K_{11} & K_{12} & K_{13} \\ K_{21} & K_{22} & K_{23} \\ K_{31} & K_{32} & K_{33} \end{bmatrix} \begin{Bmatrix} \phi_1 \\ \phi_2 \\ \phi_3 \end{Bmatrix} = \begin{Bmatrix} V_{n_1} \\ V_{n_2} \\ V_{n_3} \end{Bmatrix} \qquad (2.9)$$

e,

$$K_{ij} = \int\int \left(\frac{\partial N_i}{\partial x}\frac{\partial N_j}{\partial x} + \frac{\partial N_i}{\partial y}\frac{\partial N_j}{\partial y}\right) dx\, dy \qquad (2.10)$$

$$K_{ij} = K_{ji}, \quad i,j, = 1,2,3.$$

The interpolating functions for an element are

$$N_1 = \frac{1}{2\Delta^e} (X_2Y_3 - X_3Y_2) + X(Y_2-Y_3) + Y(X_3 - X_2)$$

$$N_2 = \frac{1}{2\Delta^e} (X_3Y_1 - X_1Y_3) + X(Y_3 - Y_1) + Y(X_1 - X_3)$$

and

$$N_3 = \frac{1}{2\Delta^e} (X_1Y_2 - X_2Y_1) + X(Y_1-Y_2) + Y(X_2 - X_1)$$

where,

$$\Delta^e = \frac{1}{2} (X_1Y_2 - X_2Y_1) + (X_2Y_3-X_3Y_2) + (X_3Y_1-X_1Y_3) \quad . \tag{2.11}$$

After finding out element stiffness matrices $[K]^{(e)}$ and normal velocity vector for each element, they are assembled for the entire domain to get a global stiffness matrix and a global velocity vector respectively. On applying boundary conditions, given by equation (2.12),

$$\begin{aligned} \frac{\partial \phi}{\partial n} &= 0 \quad \text{along solid surfaces} \\ \phi &= 0 \quad \text{along open edge} \\ \frac{\partial \phi}{\partial n} &= V_n = \text{Velocity in the gap at the end of side zone (Figure 2.4).} \end{aligned} \tag{2.12}$$

the system will yield a set of linear equations, which could be solved for ϕ by any standard technique. Here, Gauss

elimination technique has been used.

Once the velocity potential ($\emptyset$) is obtained at each node, the velocities in stray current zone are calculated using equation (2.13).

$$U = \sqrt{u^2 + v^2} \qquad (2.13)$$

where,

$$u = \frac{\emptyset_1(Y_2-Y_3) + \emptyset_2(Y_3-Y_1) + \emptyset_3(Y_1-Y_2)}{2\Delta^e}$$

$$v = \frac{\emptyset_1(X_2 - X_3) + \emptyset_2(X_3 - X_1) + \emptyset_3(X_1 - X_2)}{2\Delta^e}$$

and Δ^e is given by equation (2.11).

2.2.2 CURRENT DENSITY (J) AND CONDUCTIVITY (K)

The current density can be determined either from Ohm's law or from potential distribution obtained by solving Laplace equation.

The application of a particular case depends upon the nature of interelectrode gap (IEG) and electric potential lines. Ohm's law can be applied only when the current lines are straight and normal to the electrode surface. But this is not true when electrodes with small radii or complex shapes are used. In such cases, the current density calculated from potential distribution obtained by solving Laplce's equation gives more accurate results. The current density at any point

on the workpiece is calculated as

$$J = K \frac{\partial \phi}{\partial n} \qquad (2.14)$$

The electrolyte conductivity, K, is a function of electrolyte temperature (T) as well as void fraction (α_v). Tipton [7] has proposed equation (2.15) for calculation of electrolyte conductivity, which takes into account the effect of electrolyte temperature and hydrogen gas liberation.

$$K = K_i (1 + \alpha . \Delta T) (1 - \alpha_v)^n \qquad (2.15)$$

where,

K_i is the initial electrolyte conductivity and α is the temperature coefficient of electrical conductivity of electrolyte.

In equation (2.15), Hopenfeld and Cole [11] assumed a value of void fraction exponent, n = 1.5 for the case of uniform void distribution. For the case of non-uniform void distribution, especially where bubbles are concentrated near cathode, Thorpe and Zerkle [23] suggested a value of n = 2.0.

In stray current zone and stagnation zone, the effect of void fraction on conductivity is neglected, hence in these zones, the electrolyte conductivity is a function of temperature alone.

2.2.3 TEMPERATURE (T)

Following assumptions have been made in deriving the equations for temperature distribution:

(i) Total heat generated is only due to Ohmic heating. The heat generated by other sources such as friction, chemical reactions etc. is negligible.

(ii) Specific heat and density of the electrolyte remains constant.

(iii) Heat transfer through the electrodes is considered to be negligible, i.e. all the heat generated is retained by the electrolyte.

(iv) The flow velocities are such that the frictional heating of fluid is negligible.

2.2.3.1 STAGNATION ZONE

In S.T. zone, S.S. zone and S.S.C. zone (Figure 2.1), the electrolyte flow is assumed to be in axial direction. The following analysis for calculation of temperature is applicable to S.T. zone, S.S. zone and S.S.C. zone. Consider an element of length dx at a distance x from the starting of S.T. zone (Refer Figure (2.2)).

By Ohm's law, current through this element is given by,

$$I = \frac{(V - \Delta V)}{y} K \, 2\pi (r_1 - y) \, dx \quad . \qquad (2.16)$$

Rate of heat generated in the element is given by

$$\dot{dH} = I^2 R_e = \frac{(V - \Delta V)^2 K \ 2\pi(r_1 - y)\ dx}{y} . \quad (2.17)$$

Rate of heat carried away by the electrolyte,

$$\dot{dH} = \dot{Q} \rho_e C_e \ dT . \quad (2.18)$$

Equating (2.18) and (2.17) yields

$$\dot{Q} \rho_e C_e \ dT = \frac{(V - \Delta V)^2 K \ 2\pi(r_1 - y)dx}{y} .$$

Using $K = K_i (1 + \alpha \Delta T)$, the expression for temperature distribution becomes,

$$\frac{dT}{1 + \alpha(T - T_i)} = A' \ dx \quad (2.19)$$

where,

$$A' = \frac{K_i (V - \Delta V)^2 \ 2\pi(r_1 - y)}{y \ \dot{Q} \rho_e C_e} .$$

Integrating equation (2.19) with boundary condition, at $x = x_{ref}$, $T = T_i$, gives,

$$T - T_i = \frac{1}{\alpha} \{[\exp \alpha A' (x - x_{ref})] - 1\} . \quad (2.20)$$

2.2.3.2 FRONT ZONE

Consider an element of thickness 'dr' at a distance r, from the axis of the tool (Figure 2.3d).

Using Ohm's law, the current I through this element is given by,

$$I = \frac{(V - \Delta V)\, K\, 2\pi r\, dr}{Y} \quad . \tag{2.21}$$

Rate of heat generated in the element is given by,

$$\dot{dH} = I^2 R_e = \frac{(V - \Delta V)^2\, K\, 2\pi r\, dr}{Y} \quad . \tag{2.22}$$

Rate of heat carried away by the electrolyte,

$$\dot{dH} = \dot{Q}\, \rho_e\, C_e\, dT \quad . \tag{2.23}$$

Equating (2.23) and (2.22) yields

$$\dot{Q}_e\, C_e\, dT = \frac{(V - \Delta V)^2\, K\, 2\pi r\, dr}{Y} \quad .$$

Using $K = K_i\,(1 + \alpha \cdot \Delta T)$, the expression for temperature distribution becomes,

$$\frac{dT}{1 + \alpha(T - T_i)} = A''\, r\, dr \tag{2.24}$$

where,

$$A'' = \frac{2\pi K_i\, (V - \Delta V)^2}{\dot{Q}\, \rho_e\, C_e\, Y} \quad .$$

The integration of equation (2.24) with boundary conditions, at $r = r_i$, $T = T_i$ gives,

$$T - T_i = \frac{1}{\alpha}\{\exp\left[A''\left(\frac{r^2 - r_i^2}{2}\right)\right] - 1\} \qquad (2.25)$$

2.2.3.3 TRANSITION AND SIDE ZONES

In these two zones, the electrolyte flow is assumed to be in axial direction. Consider an element of length dx at a distance X from the end of front zone, i.e. from X_{ref} (Figure 2.3e).

By Ohm's law,

$$I = \frac{(V - \Delta V)\, K\, 2\pi(r_2 + Y)\, dx}{Y} \,. \qquad (2.26)$$

From equation (2.26), the rate of heat generated in the element is given by

$$\dot{dH} = I^2 R_e = \frac{(V - \Delta V)^2\, K\, 2\pi(r_2 + Y)\, dx}{Y} \qquad (2.27)$$

Equating equations (2.27) and (2.23) gives,

$$\dot{Q}\, \rho_e\, C_e\, dT = \frac{(V - \Delta V)^2\, K\, 2\pi(r_2 + Y)dx}{Y} \,. \qquad (2.28)$$

or

$$\frac{dT}{1 + \alpha(T - T_i)} = A''' \, dx \qquad (2.29)$$

where,

$$A'' = \frac{2\pi K_i (V - \Delta V)^2 (r_2 + Y)}{\dot{Q} \rho_e C_e Y} \quad (2.30)$$

Integrating equation (2.29) with boundary condition at $X = X_{ref}$, $T = T_{ref}$ gives,

$$T - T_i = \frac{1}{\alpha} \{ B \exp [\alpha A'' (X - X_{ref})] - 1 \} \quad (2.31)$$

where,

$$B = 1 + \alpha (T_{ref} - T_i) \quad (2.32)$$

2.2.3.4 STRAY CURRENT ZONE

Consider an element of length 'l' at a distance r' from the axis of the tool (Figure 2.5).

By Ohm's law,

$$I = \frac{(V - \Delta V) K \, 2\pi r' \, dr'}{l} \quad (2.33)$$

From equation (2.33) the rate of heat generated in the element is given by,

$$\dot{dH} = I^2 R_e = \frac{(V - \Delta V)^2 K \, 2\pi r' \, dr'}{l} \quad (2.34)$$

Rate of heat carried away by the electrolyte is given by,

$$\dot{dH} = \dot{Q} \rho_e C_e \, dT \quad (2.35)$$

Equating (2.35) and (2.34) gives,

$$\dot{Q}\,\rho_e\,C_e\,dT = \frac{2(V-\Delta V)^2\,K\pi r'\,dr'}{l} \quad . \qquad (2.36)$$

After rearranging the terms,

$$\frac{dT}{1+\alpha(T-T_i)} = A^{IV}\,r'dr' \qquad (2.37)$$

where,

$$A^{IV} = \frac{2\,K_i\,(V-\Delta V)^2}{l\;\dot{Q}\;\rho_e\,C_e} \quad . \qquad (2.38)$$

Integrating equation (2.37) with boundary condition, at $r' = R$, $T = T_{sz}$ gives,

$$T - T_i = \frac{1}{\alpha}\left\{B_1\;\exp\left[\alpha\frac{A^{IV}}{2}(r'^2 - R^2)\right] - 1\right\} \qquad (2.39)$$

where,

$$B_1 = 1+\alpha(T_{sz}-T_i) \quad . \qquad (2.40)$$

In calculation of temperatures in Front, Transition, Side and stray current zones, initial temperature is taken to be equal to temperature at the end of stagnation zone, say, T_s. Similarly, initial conductivity of electrolyte is taken to be equal to the conductivity at the end of stagnation zone, say, K_s.

2.2.4 VOID FRACTION (α_v)

As the electrolyte flows downstream within the machining gap, due to electrolysis, hydrogen will evolve at cathode. This hydrogen evolution, usually reduces the effective conductivity of the electrolyte, so that the local anodic dissolution rate varies downstream until an equilibrium is achieved.

Considering a control volume in IEG (Figure 2.6), using the principle of conservation of mass, Thorpe and Zerkle [23] arrived at the governing differential equation, and the expression for void fraction was obtained by solving it as follows:

$$\alpha_v \approx \frac{B^* X^*}{1 + B^* X^*} \qquad (2.41)$$

where,

$$B^* = \frac{\rho_e E_g}{\sigma \rho_g E_a},$$

$$X^* = \frac{X}{LS} \quad \text{for rectilinear flow,}$$

$$X^* = \frac{X(r_i + X/2)}{LS\, r_i} \quad \text{for radial flow}$$

and

$$S = \frac{\rho_i Y_i U_i}{L \rho_a f}.$$

Here, E is the electrochemical equivalent and the suffixes a, e and g stand for anode, electrolyte and gas respectively.

In the present case, the gas slip ratio σ in the variable B^* is assumed to be unity, i.e., velocity of gas is same as that of velocity of electrolyte.

The effect of void fraction on conductivity has however been neglected in the stray current zone and stagnation zone due to the mathematical complexity of the problem.

2.2.5 ELECTROLYTE PRESSURE (P)

The electrolyte pressure [1] required to maintain the rate of electrolyte flow in a particular gap is given by

$$P = P_1 + P_2 \qquad (2.42)$$

where, P_1 is the pressure required to over come inertia force and P_2 is the pressure required to overcome viscous force.

The expressions for P_1 and P_2 are different for laminar and turbulent flows. The type of flow in the IEG can be determined from Reynold's number (R_n), given by,

$$R_n = \frac{\rho_e u_e D}{\mu_e} \qquad (2.43)$$

where, μ_e is the viscosity of the electrolyte and D is the hydraulic mean diameter which is given by,

$$D = \frac{4 \times \text{Area of cross section}}{\text{Wetted perimeter}} .$$

For a cylindrical tube, D = d, for a rectangular channel of depth Y, D = 2Y and for the case in which fluid is flowing through the annulus, D $(d_1 \quad d_2)$.

For the laminar flow ($R_n < 2000$) with a parabolic velocity distribution, the pressures P_1 and P_2 are given by

$$P_1 = \frac{1}{2} \rho_e U_e^2$$

and

$$P_2 = \frac{32 \mu_e U_e X}{d^2} , \qquad (2.44)$$

for a narrow tube of diameter d.

The flow is usually turbulent ($R_n > 2000$) in ECM. From Bernouli's equation,

$$P_1 = \frac{1}{2} \rho_e U_e^2 .$$

The value of P_2 is given by Blasius equation,

$$P_2 = \frac{0.3164 \rho_e U_e^2 X}{2D R_n^{0.25}} \qquad (2.45)$$

The pressure P_2, in turbulent flow is a function of Reynold's number. At high Reynold's number inertia force will be more than the viscous force which results in higher value of P_1.

2.2.6 FEED RATE (f)

In electrochemical drilling, as the machining progresses, the side zone becomes tapered and it no longer remains a zero feed rate case. For the calculation of IEG in the side zone, the feed rate vector normal to the work surface should be

considered, as given by equation (2.46)

$$f_n = f.\cos\theta \qquad (2.46)$$

where, θ is the angle of inclination between the feed direction and normal to the work surface. The values of 'θ' for each element in the side zone and transition zone are calculated separately.

If Y_1 and Y_2 are the interelectrode gaps in side zone at points 1 and 2 respectively (Figure 2.7), then the angle θ at the point 2 is given by equation (2.47).

$$\theta = \tan^{-1} \left(\frac{X_2 - X_1}{Y_2 - Y_1}\right) . \qquad (2.47)$$

In the transition zone, the angle θ at any point is given by the intersection angle between the normal drawn at a point and the tool feed direction (Figure 2.7).

In stagnation zone analysis, equations (2.46) and (2.47) have been used for calculating the feed rate in stagnation-side zone (Figure 2.1). Since stagnation-transition zone is similar to transition zone, feed rate in stagnation-transition zone has been calculated on the same lines as feed rate in transition zone. Unlike the other zones, in stray current zone feed rate does not play a role in determining the anode profile and is hence ignored.

2.2.7 INTERELECTRODE GAP (IEG)

Electrochemical reactions would attain an equilibrium only after 't' approaches infinity and IEG can be computed from equations (2.48) and (2.49) while machining with zero feed rate and finite feed rate [1] respectively.

$$Y = (Y_o^2 + 2Ct)^{1/2} \qquad (2.48)$$

where,

$$C = \frac{AK(V - \Delta V)}{Z \rho_w F}$$

and

$$t = \frac{1}{f}\left[(Y_o - Y) + \ln\left(\frac{Y_o - Y_e}{Y - Y_e}\right)\right] \qquad (2.49)$$

Equation (2.49) is an implicit equation and can be solved by iteration process. Equation (2.48) predicts an infinite value of the gap as t approaches infinity. However, in practice, as the IEG increases, the current decreases, so that the MRR gradually decreases and for a very large gap the process would come to a stand still.

For a very small interval of time Δt, Jain and Pandey [13] derived an equation (2.50) for determining IEG which holds good for both, zero and finite feed rate.

$$Y = Y_o + (C' - f)\,\Delta t \qquad (2.50)$$

where,

$$C' = \frac{\eta J A}{\rho_w F Z} .$$

Equation (2.50) is based on the assumption that the current density 'J' remains constant over a small element of length, dX and for a small interval of time, Δt. This equation yields values of Y which are very close to those obtained from equations (2.48) and (2.49) and agree well with experimental data [3]. In the present work equation (2.50) has been used.

2.2.8 CURRENT EFFICIENCY (η)

In deriving the expression for metal removal rate by Faraday's laws of electrolysis, current efficiency was assumed to be 100%. But in actual machining process, the MRR depends on the current efficiency achieved [1], i.e., the proportion of total current that is used for the removal of metal from the anode. The current efficiency is given by,

$$\eta = \frac{\text{Actual metal removed}}{\text{Theoretical metal removed}} \times 100\% \qquad (2.51)$$

In actual practice, the values of current efficiency may be higher or lower than 100% depending on the conditions of machining. Current efficiency values less than 100% are obtained because of the side reactions at the anode, e.g., evolution of oxygen gas or Fe^{+++} ions instead of Fe^{++} ions etc.

If the dissolution of the anode occurs at a valency lower than the one used for calculation, the current efficiency obtained may be higher than 100%. Moreover, selective dissolution may occur at the material irregularities such as at grain boundaries [24] and hence may cause removal of chunks of material. In this case, the actual material removed is more than the theoretical one, which results in current efficiency higher than 100%.

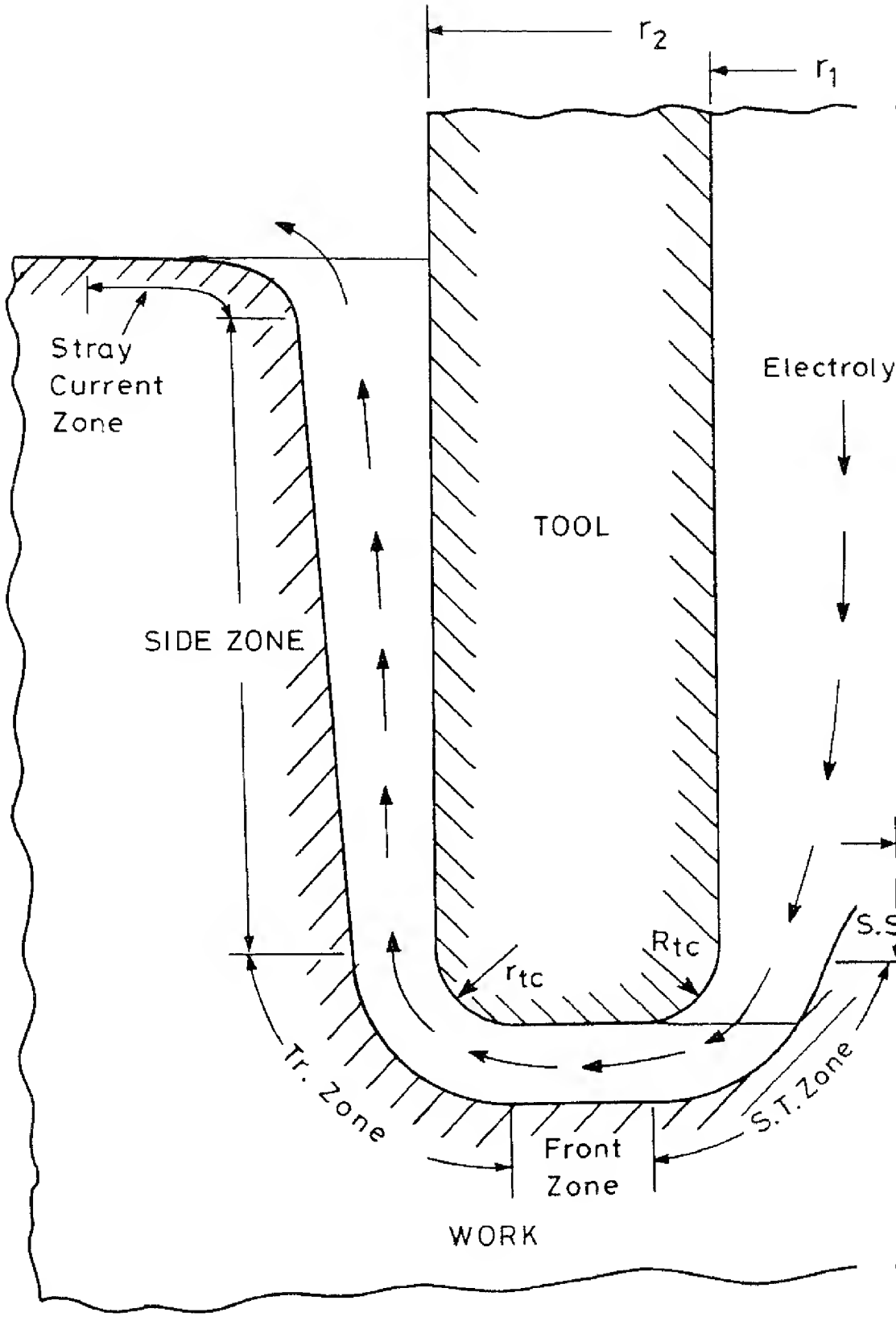

Tr. Zone – Transition Zone
S.T. Zone – Stagnation - Transition Zone
S.S.C. Zone - Stagnation - Stray Current Z
S.S. Zone – Stagnation - Side Zone

Fig. 2.1 Various zones in ECD

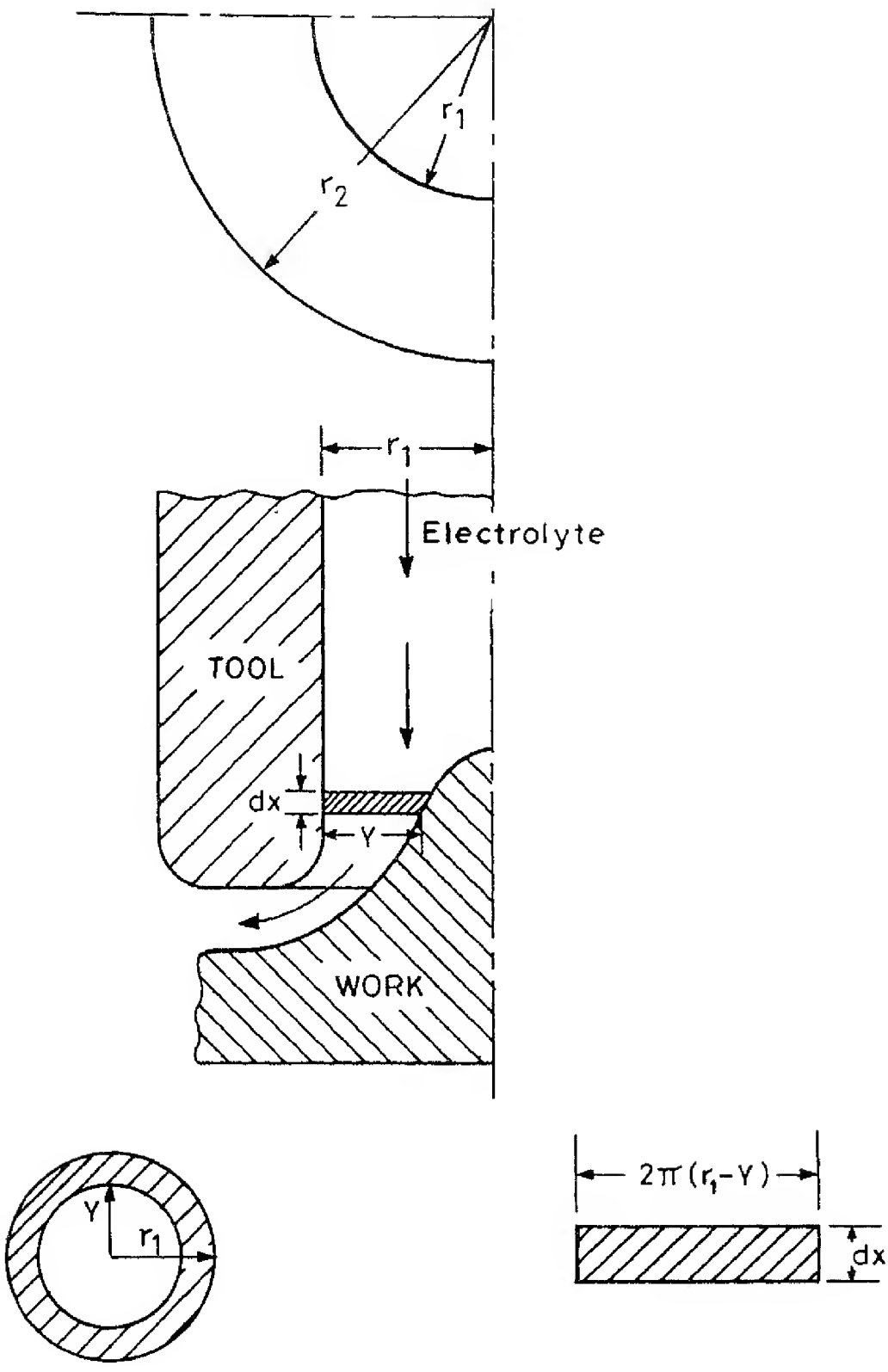

(a) Electrolyte Flow Area (b) Current Flow Area

Fig. 2.2 Electrolyte and current flow area in stagnation zone for outward mode of electrolyte flow.

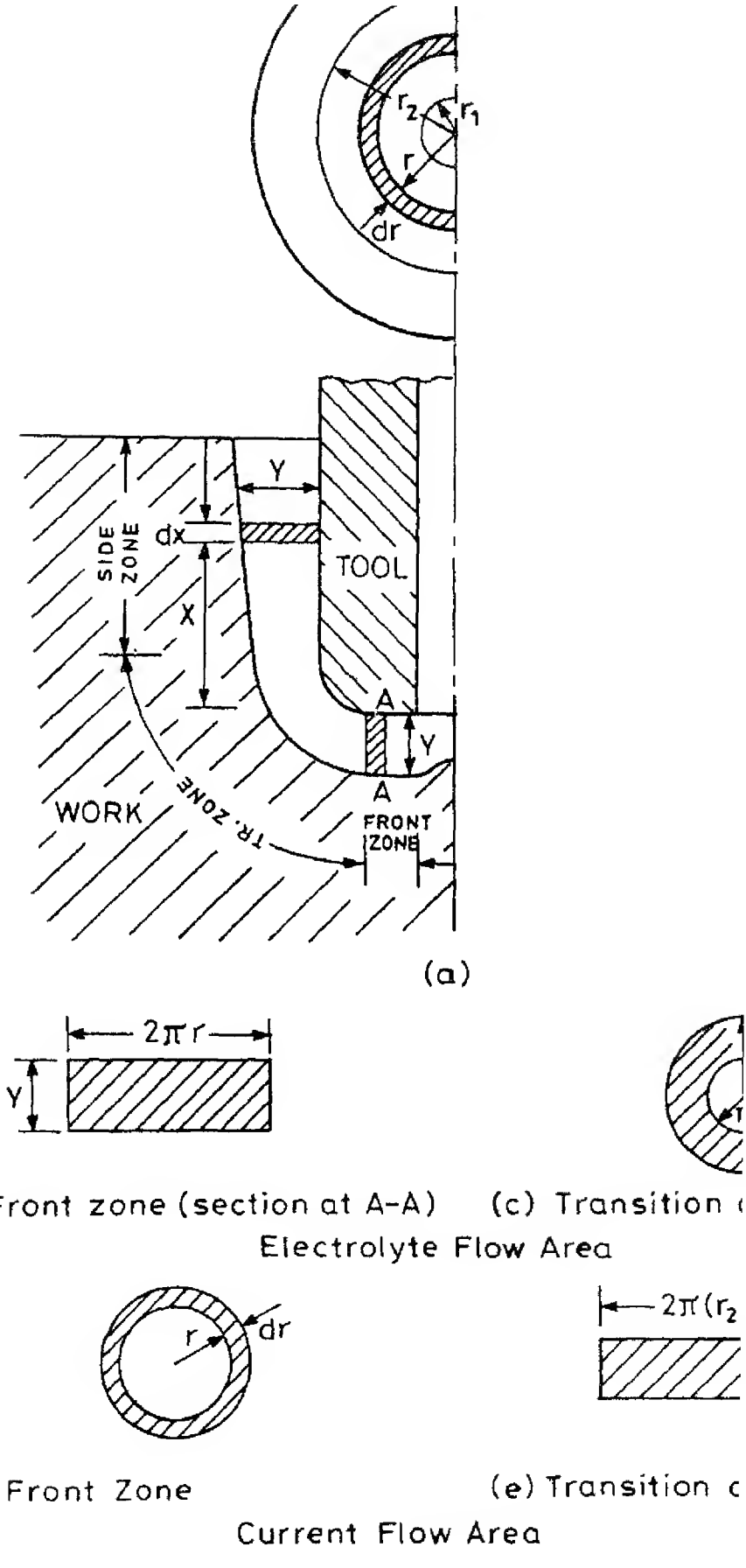

Fig. 2.3 Electrolyte and current flow area in transition and side zones.

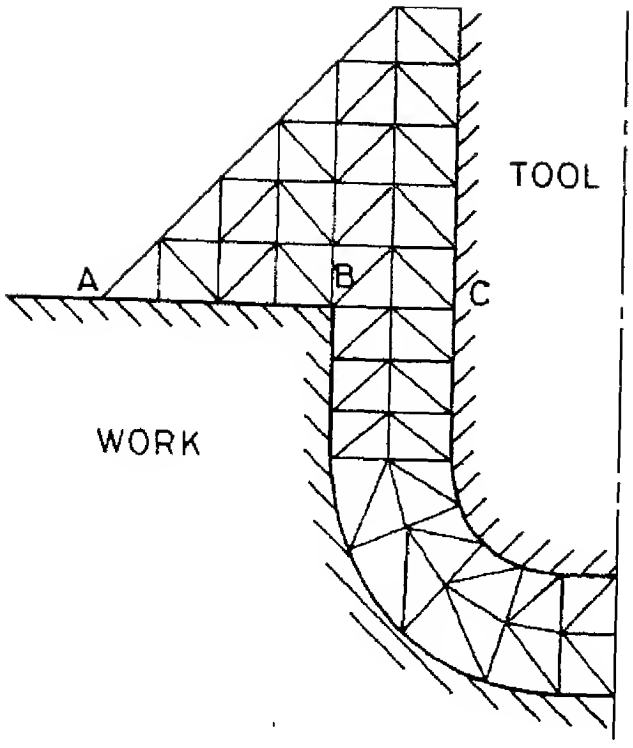

Boundary	Condition
AD	$\phi = 0$
AB, CD	$(\partial\phi/\partial n) = 0$
BC	$(\partial\phi/\partial n) = V_n$

Fig. 2.4 Finite element discretization & velocity boundary conditions in stray current zone.

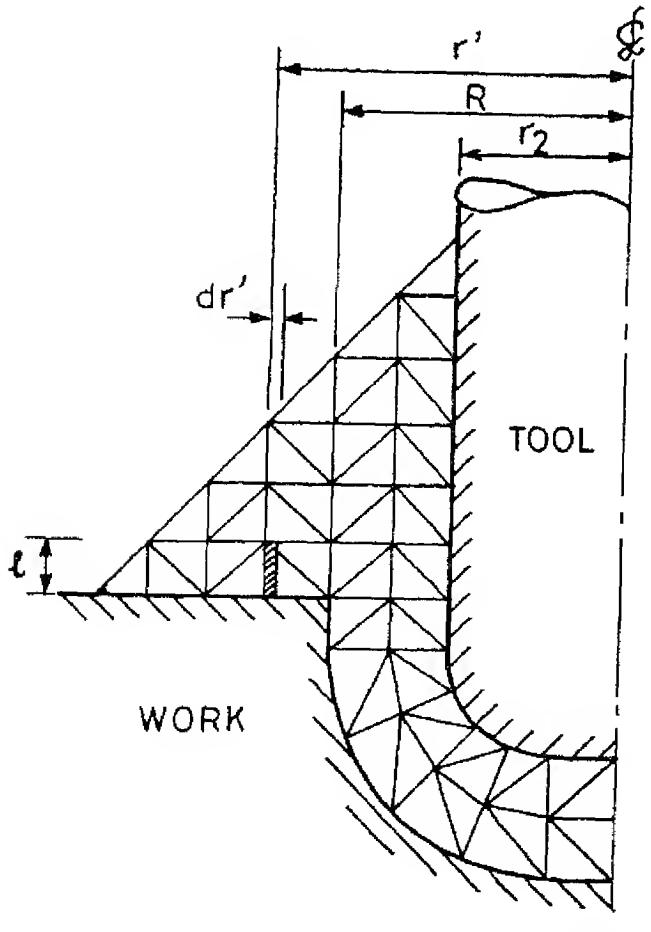

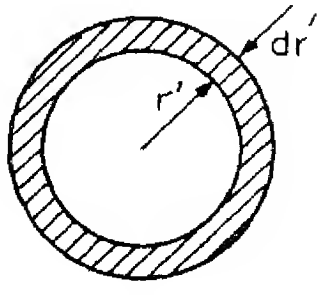

Fig 2.5 Current flow area in stray current zone for outward mode of electrolyte flow

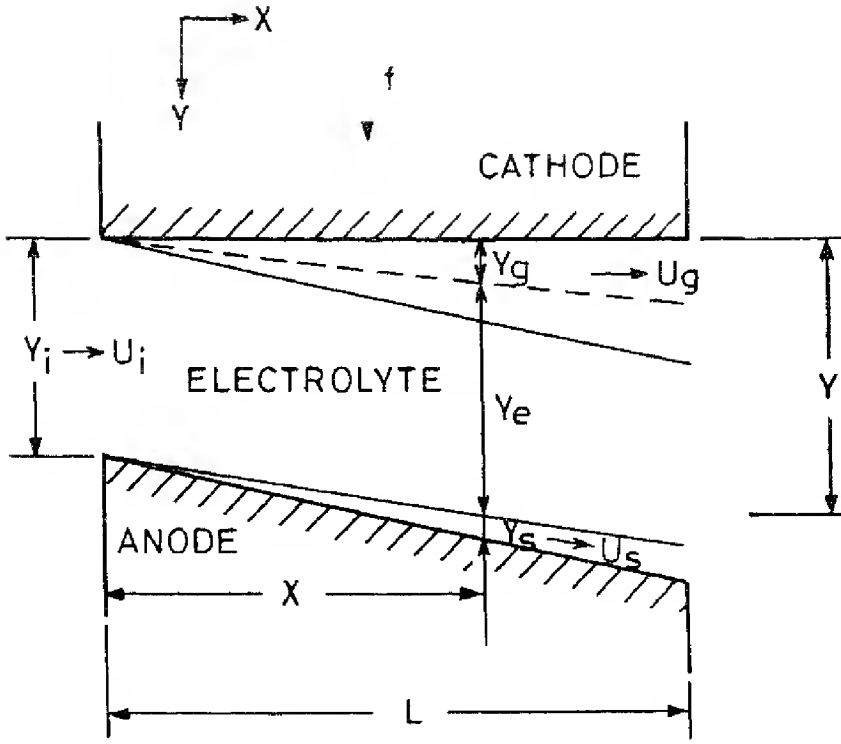

Fig. 2.6 Variation in gap width along electro
flow direction [23]

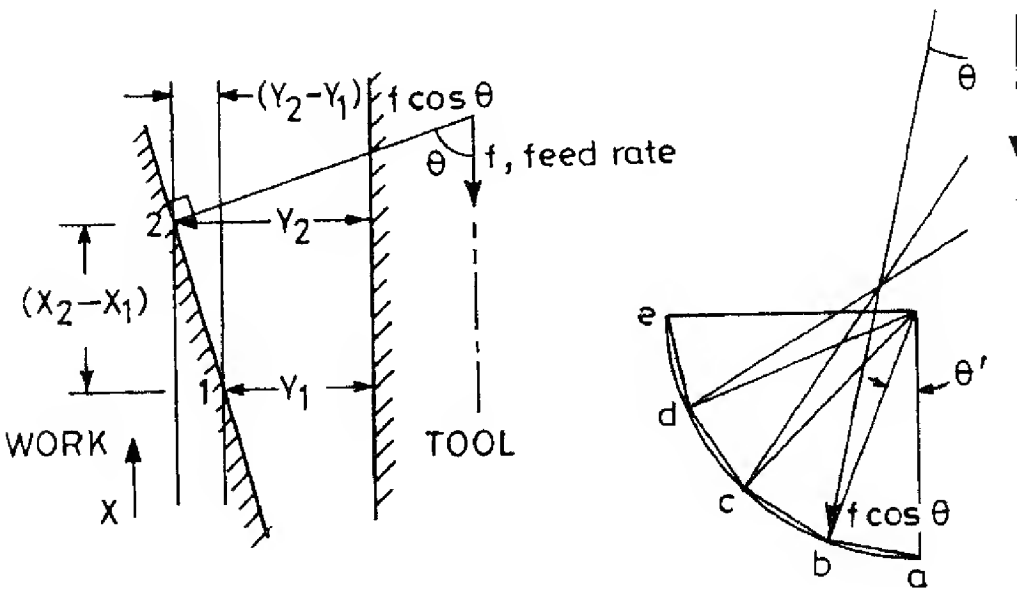

Fig. 2.7 Feed rate components in side and t
tion zones [15]

CHAPTER III

TOOL DESIGN

3.1 INTRODUCTION

Electrochemical drilling is a process of making holes of any shape and size using the principle of controlled anodic dissolution. The electrolytic cell for an ECD process is illustrated in Figure (3.1). The cathode is simply a straight tube, shaped for obtaining the desired work geometry. The electrolyte is carried to the drilled hole in the work-piece (anode) through the tool, and metal removal takes place as the electrode is fed in the downward direction.

3.2 PREDICTION OF ANODE SHAPE

For the purpose of analysis of the process, the entire machining region has been divided into five zones (Figure 3.2), namely, stagnation, front, transition, side and stray current zone. To reduce the complexity in the present problem, the stagnation zone has been analysed separately from the other four zones. Further, depending upon the location of inlet and outlet of electrolyte, the electrolyte flow mode can be classified as outward, inward or side flow.

In the present work, the finite element technique has been applied to the circular hole drilling with bare tool for outward mode of electrolyte flow. Anode shape prediction model developed by Jain and Yogindra [15] has been modified to

predict the anode shape in all the five zones mentioned above. In the anode shape prediction model developed here (STZFET-22), the field distribution is obtained by solving the Laplace equation ($\frac{\partial^2 \phi}{\partial x^2} + \frac{\partial^2 \phi}{\partial y^2} = 0$) with the following boundary conditions:

(i) $\phi = 0$ along cathode (tool)

(ii) $\phi = (V - \Delta V)$ along anode (work)

(iii) $\frac{\partial \phi}{\partial n} = 0$ (along open edges).

Since ECD is a moving boundary problem, the domain shape and size will change after each computational machining cycle time, Δt sec. As the tool penetrates in the work surface, the total number of nodes would also increase. The coordinates of each node, therefore should be recomputed after each computational cycle. Figure (3.3) shows the finite element discretization and renumbering of nodes after one computational cycle in all the zones except stagnation zone. Figure (3.4) illustrates the same for stagnation zone analysis. Here, an assumption has been made that the feed to the tool is given only after machining has taken place for a time period of Δt seconds, i.e. the process is considered as intermittent cutting rather than continuous one, as in actual ECM.

Due to complex nature of ECM process, majority of models proposed for anode shape prediction in ECD, do not

account for the simultaneous variations in the process parameters such as temperature, conductivity etc. It is felt that for an accurate prediction of anode profile, the variations in all these process parameters with machining time and their effect on anode profile should be considered. These aspects have been included in the present model, STZFET-22. Some problems have been attempted using STZFET-22 and the predicted anode profiles have been compared with experimental anode profiles.

3.3 TOOL (CATHODE) DESIGN FOR ECD

The problem of designing a tool to produce a required work shape is probably the single most important problem in ECM, and in practise, methods of design are still empirical even to the point of 'trial and error'. The IEG between tool and work is a function of various machining parameters. Hence, the tool shape is not congruent with the work shape in the strict sense. The ECM tool design depends essentially on the accuracy of the corresponding anode shape prediction model. Therefore, for accurate tool-design is ECM, the anode shape prediction model must account for the variations in process parameters while arriving at an anode shape.

Reddy [25] has suggested a 'Correction Factor Method' for tool design in ECM. In this chapter, a two dimensional

model for predicting a cathode configuration which can produce specified anode shape under prescribed machining conditions has been described. This model has been suggested by Ravi Raju [16] and has been modified here to include stray current zone and stagnation zone. The anode shape prediction model (STZFET-22) described earlier has been used for tool design in ECD. This model has been suitably modified for the prediction of work-shape with a tapered tool.

3.4 GENERAL DESIGN PROCEDURE

Tool design procedure for producing the required work shape while machining under given conditions is summarized below:

STEP 1 - INITIAL TOOL SHAPE

The first step is to assume a tool shape depending on the required work shape. For majority of the cases, the tool shape can be assumed as congruent to the desired work shape.

STEP 2 - WORK SHAPE PREDICTION

The second step is to predict the work shape obtainable from the tool shape assumed in the first step. Out of the many models available for anode shape prediction in ECM, the models based on numerical methods like FDM and FEM, can predict the work profiles reasonably accurately.

STEP 3 - ERROR AND CORRECTION

The third step is to compare the predicted work shape with the required work shape and to obtain deviations

between them. If the deviation is more than the specified tolerance, correction required to minimise this error has to be calculated.

STEP 4 - MODIFICATION

The fourth step is to modify the present tool shape by applying the correction appropriately. Using this modified tool, again the anode shape is predicted. Steps 2,3 and 4 are repeated till the predicted work shape with the desired tolerance is obtained.

This is an iterative process and the flow chart for this process is shown in Figure (3.6). Tool shape is refined progressively in each design cycle. Finally, it will give the tool shape which produces the desired work shape.

From the above mentioned procedure, it is evident that any inaccuracy associated with the anode shape prediction model will be reflected on the designed tool shape .

3.5 TOOL DESIGN FOR ECD

Here, an attempt has been made to design bare tool for electrochemical drilling. Here, a case of only cylindrical hole (straight sided and tapered both) drilling has been considered. However, the model can be applied with slight changes, to drilling of non-cylindrical holes as well. Using above mentioned procedure the tool design model developed by Ravi Raju [16] has been modified to incorporate the tool design

for stray current zone and stagnation zone. Details of the above mentioned steps for the present model are as given below.

3.5.1 INITIAL TOOL SHAPE

Initial tool shape has been assumed as a cylindrical one, with its radius equal to 1 mm lesser than the required hole radius for the case of tool designed for uniform diameter hole drilling. In transition zone, tool corner radius is again assumed as 1 mm lesser than the required work surface radius in the transition zone. This 1 mm value has been chosen arbitrarily, and any other value could as well be chosen.

3.5.2 PREDICTION OF ANODE SHAPE

The anode shape prediction model discussed in the earlier section has been used for computing the anode profile. The IEG's at the beginning of a computational cycle get modified in the following cycle. Also, the tool occupies a new position after each computational machining cycle. The modified coordinates are assigned to the corresponding points on tool and workpiece, to obtain the correct work shape at the end of a computational cycle.

3.5.3 CALCULATION OF ERROR AND CORRECTION

The coordinate system for the five zones namely stagnation, front, transition, side and stray current zones is shown in Figure (3.5). The system of coordinates has been so chosen that the same error calculation principle holds good

for all the five zones. The error and correction at each node are calculated as follows:

$$\text{ERROR (I)} = \text{OWS (I)} - \text{RWS (I)} \qquad (3.1)$$

$$\text{CORR (I)} = -\text{ERROR (I)} \qquad (3.2)$$

where,

CORR (I) = Correction to be made at I^{th} node.

OWS (I) = Obtained work shape at I^{th} node.

The obtained work shape at any node in front, transition, side zones and, S.T. zone and S.S. zone of stagnation zone is represented by Y co-ordinate of that node. However, in stray current zone and S.S.C. zone of stagnation zone, the obtained work shape at any node is given by the X coordinate of that node.

RWS (I) = Required work shape at I^{th} node.

For representing the required work shape at any node the same argument given above for obtained work shape in different zones holds good.

The correction need not always be equal to error in all design cycles. It can be calculated from the trend of the previous design cycle. It may sometimes consume less CPU time [16] . From the second design cycle onwards, the correction may be calculated as given below.

$$CORR_K(I) = \frac{CORR_{K-1}(I) \times ERROR_K(I)}{ERROR_{K-1}(I) - ERROR_K(I)} \qquad (3.3)$$

where, suffix K stands for the present design cycle and suffix K-1 stands for the previous design cycle.

However, for the sake of simplicity, in the present work, equation (3.2) has been used.

3.5.4 MODIFICATION

The tool that has been used in the previous design cycle is modified by applying correction to Y coordinates of the tool at different nodes. The new tool shape is given by equation (3.4).

$$NTS(I) = Y(I) + CORR(I) \qquad (3.4)$$

where,

NTS(I) = Y coordinate of new tool shape at the I^{th} node

Y(I) = Y coordinate of tool in previous cycle.

Correction at any node (CORR (I)) may be positive or negative depending on the deviation between the obtained work shape and required work shape at a particular node.

Unlike plane parallel electrodes ECM, in ECD a node on the workpiece is exposed to different nodes on tool for different

times. Thus, if a tool shape at a node is changed, it will affect the work shape at many other nodes on its way. This in addition to the complex nature of ECM owing to electrochemical, thermal and hydrodynamic factors, makes the tool designing more difficult in ECD with bare tool. The former problem, to some extent, is eliminated in case of electrochemical bit drilling.

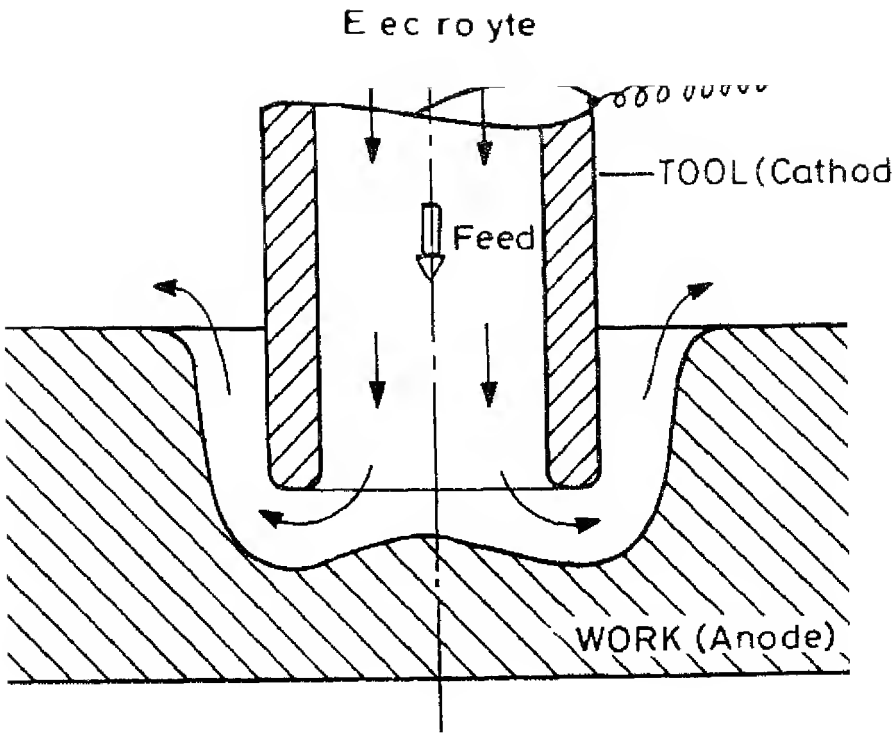

Schematic diagram of ECD with outward
of electrolyte flow.

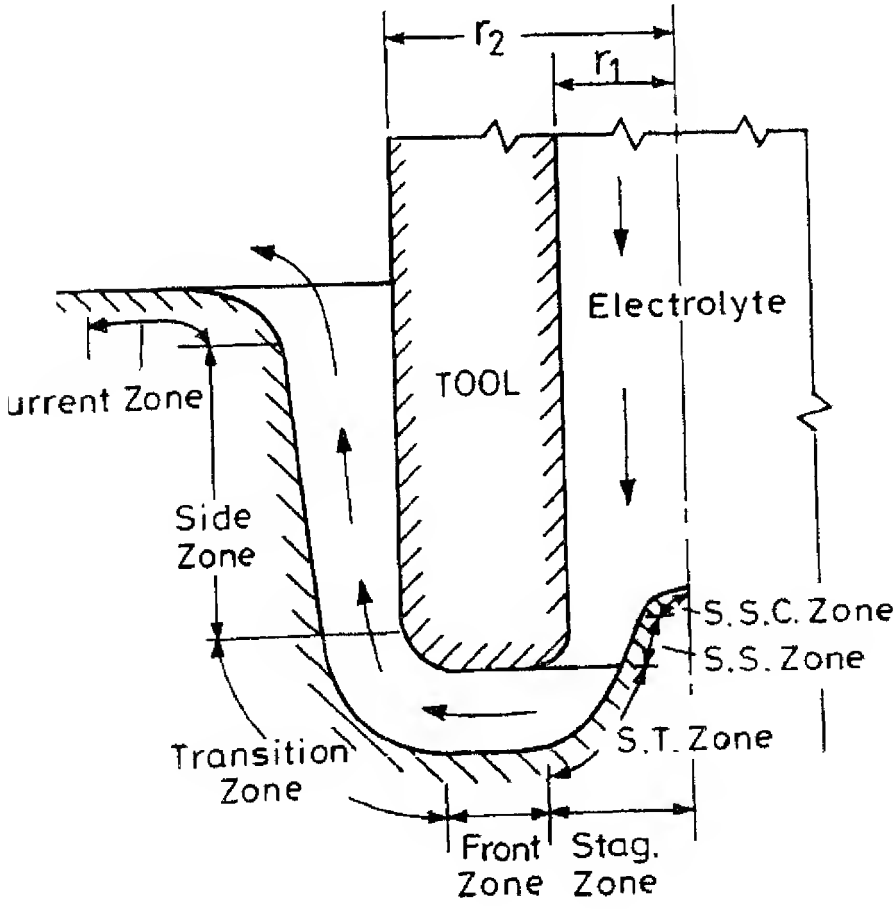

2 A complete picture of various zones i

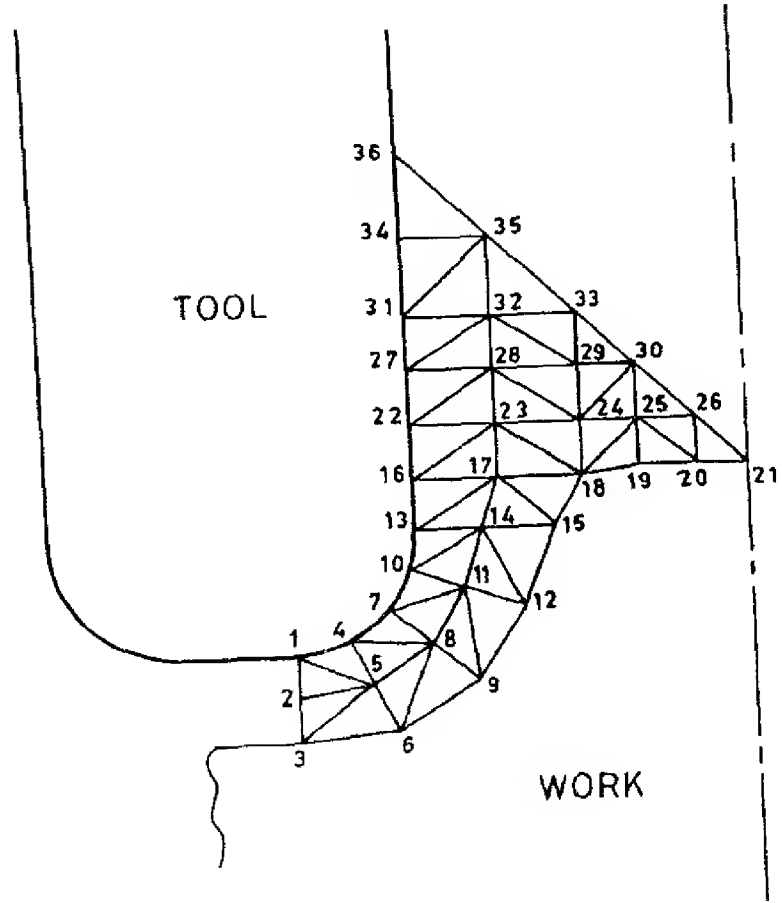
TOOL
WORK
1
2
3
4
5
6
7
8
9
10
11
12
13
14
15
16
17
18
19
20
21
22
23
24
25
26
27
28
29
30
31
32
33
34
35
36

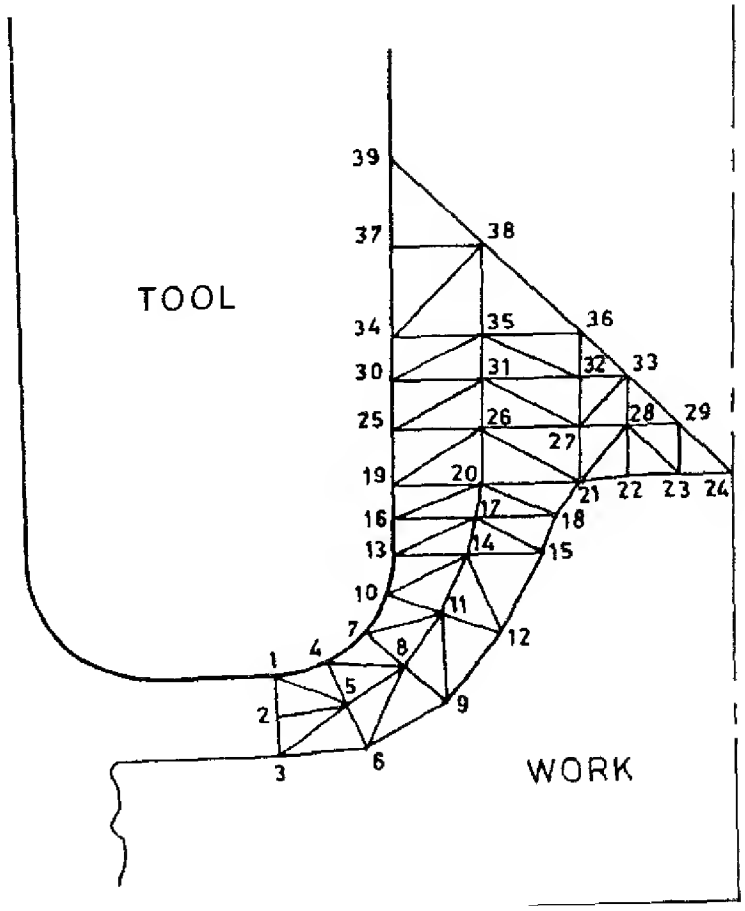
TOOL
WORK
1
2
3
4
5
6
7
8
9
10
11
12
13
14
15
16
17
18
19
20
21
22
23
24
25
26
27
28
29
30
31
32
33
34
35
36
37
38
39

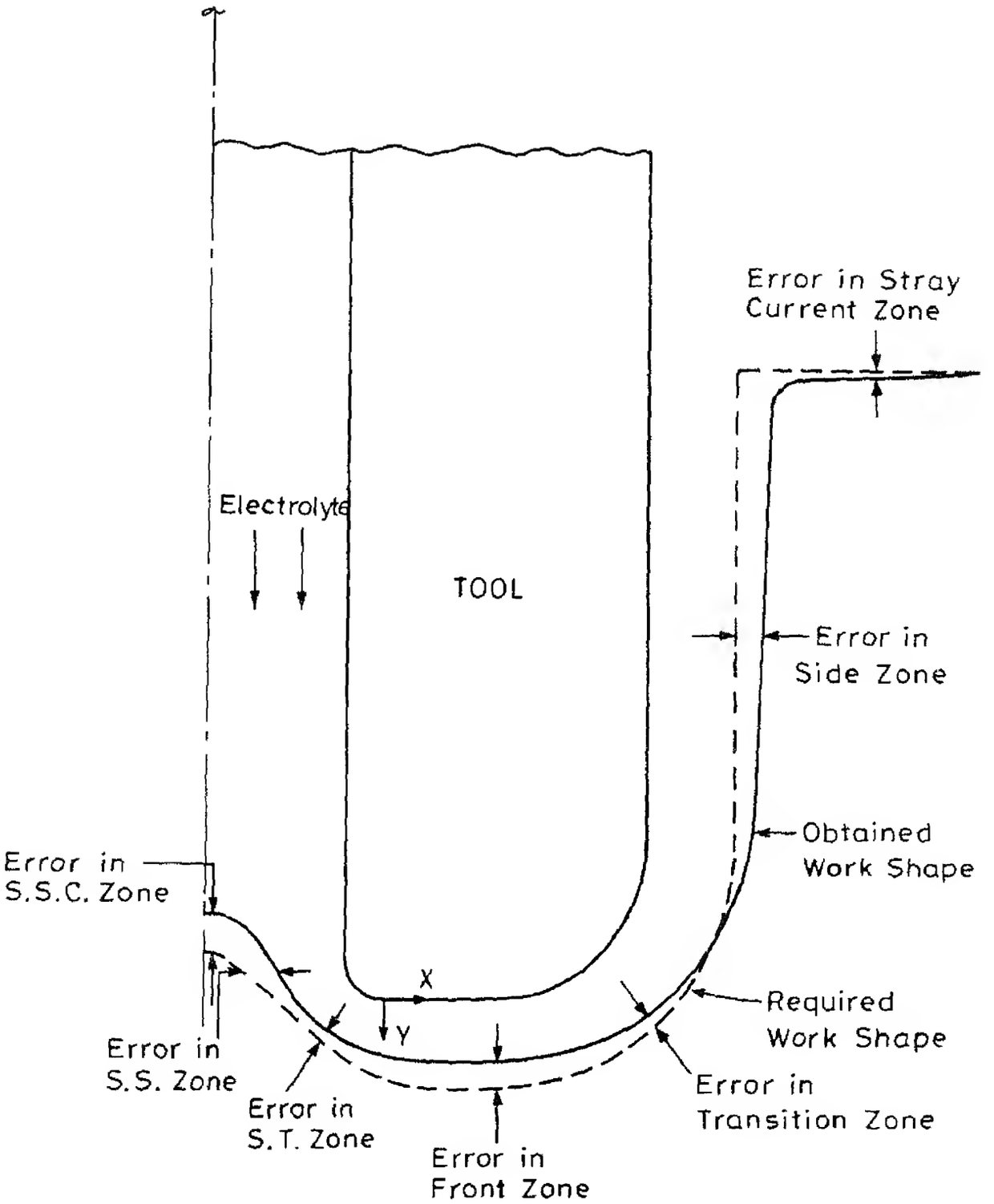

Fig. 3.5 Error representation in ECD.

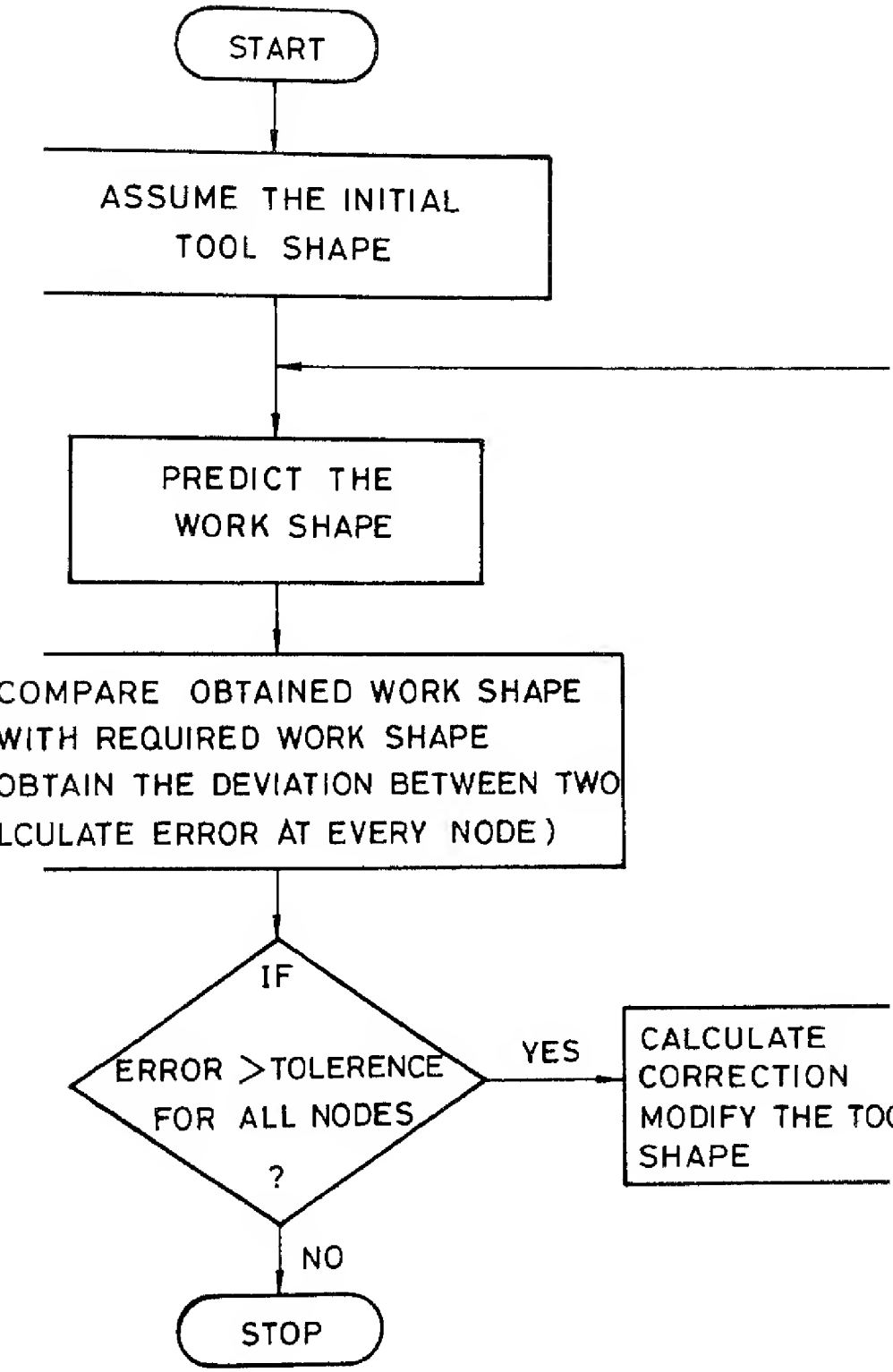

.6 FLOW CHART FOR GENERAL DESIGN PRO

CHAPTER IV

RESULTS AND DISCUSSIONS

To ascertain the validity of any analytical model, it is essential to compare the analytically obtained results with the experimental data. With this basis in mind, in this chapter, a comparison between the analytical and experimental anode profiles obtained during ECD with bare tools has been made. Also, the tools designed for producing the experimentally obtained anode profiles and the tools used during experimentation have been compared. However, since experimental work profile in the stagnation zone is not available it could not be compared with the analytically obtained work profile in the stagnation zone. Further, because of this, part of the tool designed for obtaining a desired work shape in stagnation zone could not be compared with tool used during experimentation.

Jain [3] conducted experiments using brass as material for tools and low alloy steel castings and low alloy steel forgings as materials for anodes (Table - 1). The machining conditions for ECD experiments are given in Table - 2. The shape and size of anode profiles were measured by preparing a cast replica of a drilled hole, and projecting it on a tool maker's microscope. The method by which anode corner radius was measured, has been described in detail in reference [3].

For analytical computation of anode profile, modified equation (2.50) suggested by Jain [3] has been used.

4.1 ANODE SHAPE PREDICTION

Using the model STZFET-22 discussed earlier, anode profiles for different machining conditions have been obtained, assuming constant valency of electrochemical dissolution of the anode and taking a mean value for the efficiency of machining (Table - 3). Voltage fluctuation history (Table - 4) has also been used while computing the anode profiles. This would obviously predict more accurate anode profile unlike the case in which mean voltage is used, since during experimentation voltage was varying rather than remaining constant. The anode profile obtained for stagnation zone by model STZFET-22 has been superimposed on that obtained for other four zones so as to get the profi for all the five zones (Figure 3.2). These profiles for different machining conditions have been shown in Figure (4.1).

It can be seen from Figure (4.1) that in majority of the cases, the electrochemically drilled holes have the shap of an elongated S(∫). The large overcut at and near the t surface of the workpiece is attributed partly to the stray current attack and partly to the fact that this section of t

workpiece has been subjected to electrochemical dissolution throughout the period of ECD. A good quantitative agreement between theoretically predicted and experimentally obtained anode profiles was observed (Figure 4.1). The small deviations between the analytical and experimental anode profiles in front, transition, side and stray current zones are due to the following reasons:

(i) The valency of dissolution plays an important role in determining the shape and size of the computed anode profiles. The present analytical model assumes some constant value of valency of dissolution. But in actual machining, the valency of dissolution may be greater than the assumed one [26] and hence the assumed lower valency would result in larger computed overcut. In the present work, valency of electrochemical dissolution has been assumed to be 2. But as reported in [26] for the conditions prevailing in present case of ECD, iron may dissolve with a valency of 3 instead of 2. This would reduce the overcut and thereby narrow the deviation between the experimental and analytical anode profiles.

(ii) The electrolyte conductivity within the IEG is a function of both temperature and void fraction as given by equation (2.15). The value of exponent 'n', in equation (2.15), depends on the nature of distribution of voids in the IEG. For uniform void distribution,

Hopenfeld and Cole [11] suggested a value of n = 1.5, and for non-uniform void distribution, especially when bubbles are concentrated near the cathode, Thorpe and Zerkle [23] suggested a value of n = 2.0. But in actual machining, it is extremely difficult to know the exact void distribution. Owing to this reason, an average value of n = 1.75 has been assumed for computing void fraction. This approximation might also have contributed to some error in calculation of overcut. In stray current zone, the void fraction has been ignored, to keep the problem mathematically tractable, and hence the conductivity is assumed to be a function of temperature alone. This may also lead to some variation between analytical and experimental anode profiles in stray current zone.

(iii) In some of the tests, due to sparking or some other unavoidable reasons, the machining had to be stopped and the IEG readjusted. This would change both the current and voltage variation history and hence would lead to deviations between predicted and experimental anode profiles.

(iv) In the present analytical model, no consideration has been given to the effects of grain size, grain boundary attack, selective dissolution of various alloy components, and other metallurgical aspects. This is expected to affect the value of computed overcut.

Since no experimental results are available about the spike profile in the stagnation zone, the analytically predicted anode profile in this particular zone could not be compared. However, the analytically obtained spike profile seems to be some what larger than the one that could have been normally expected. This discrepancy can be assigned to the following reasons:

(a) Reason (i) mentioned above.

(b) No consideration for the effect of void fraction on conductivity. Conductivity has been assumed to be a function of temperature alone.

(c) Use of simple triangular elements in finite element discretization of the stagnation zone which may not fit exactly with the work or tool boundary, leading to an error.

4.1.1 COMPARISON BETWEEN THE MODELS STZFET-22 and SBFET-11

From Figure (4.1), it is evident that the model STZFET-22 gives better agreement with experimental anode profiles in front, transition and side zones, as compared to those obtained from SBFET-11. Also, the model SBFET-11 is incapable of predicting the anode profile in the stray current zone and stagnation zone. The model SBFET-11 is a one-dimensional model and is based on the assumption that the lines of electric flux are straight and normal to the

electrode surfaces. The current density in the IEG is calculated from the Ohm's law. But in complex shaped workpiece, especially at curved sections, the electric flux lines are not straight (Figure 1.5) and hence Laplace equation has to be solved to get accurate potential distribution in the domain of interest. In the model STZFET-22, current densities at different nodes are calculated from potential distribution obtained by solving Laplace's equation. That is why, anode profiles predicted by STZFET-22 are more accurate than the profiles predicted by SBFET-11.

The accuracy of the results obtained by finite element technique also depends on the type of elements selected for discretization of the solution domain. The model STZFET-22 uses two dimensional triangular elements, which fit better in the curved boundaries, as compared to one dimensional linear elements used in model SBFET-11. This also contributes to the better accuracy of model STZFET-22. However, use of isoparametric elements would further increase the accuracy of computed results.

4.1.2 EFFECT OF TEMPERATURE AND VOID FRACTION ON CONDUCTIVITY

Figure (4.5a) shows the variation in temperature, and void fraction and conductivity along the electrolyte flow path distance. The magnitude of increase in temperature is not much. From Figure (4.5a) it can be seen that the effect

of void fraction on electrolyte conductivity is more significant than that of temperature rise. The electrolyte conductivity decreases drastically with the electrolyte flow distance. For clarity, the variation in temperature and conductivity along the electrolyte flow path in stray current zone is shown separately in Figure (4.5b). It should be noted that in stagnation zone and stray current zone, the effect of void fraction on conductivity is neglected. Hence, in these zones the electrolyte conductivity is a function of temperature alone.

4.2 CATHODE DESIGN

Figure (4.2) shows a comparison between tool shape designed by correction method and the tool shape used during experimentation for the case of ECD with bare tools, under different machining conditions. Here, the required and obtained work shapes are coinciding because the design procedure is continued till the deviation between the required and obtained work shapes lie within an accuracy of 10 μm. There is a good agreement between the designed and experimental tool used under the same machining conditions. Kinks, just opposite to the unevenness in the experimental profile, are observed in the designed tool shape. This is particularly observed at the end of transition zone.

Figure (4.2) also shows the tool designed by Ravi Raju [16] using model DES-22. The tools designed by model STZDES-22 and

model DES-22 show a close agreement between the two. However, the model DES-22 is incapable of predicting the tool shape by taking into consideration the stray current effect.

Figure (4.3) shows the designed bare tool (using model STZDES-22) for producing a straight sided hole with top surface of the workpiece square with the hole walls (i.e. the top surface of the workpiece is flat and has not undergone any damage due to stray current attack). The tool shapes designed by model DES-22 have also been plotted for comparison (Figure 4.3). Once again, the stray current zone has been neglected in model DES-22.

Figure (4.4) shows the designed tool (with an uninsulated bore) for obtaining the desired spike profile. The desired spike profiles for different problems have been shown in Figure (4.4). It should be noted that the model STZDES-22 is capable of designing the electrolyte hole profile for any desired spike profile. In the present work, the spike profile has been chosen such that it is similar in nature to the spike profile obtained by experimental tool, but lesser in height.

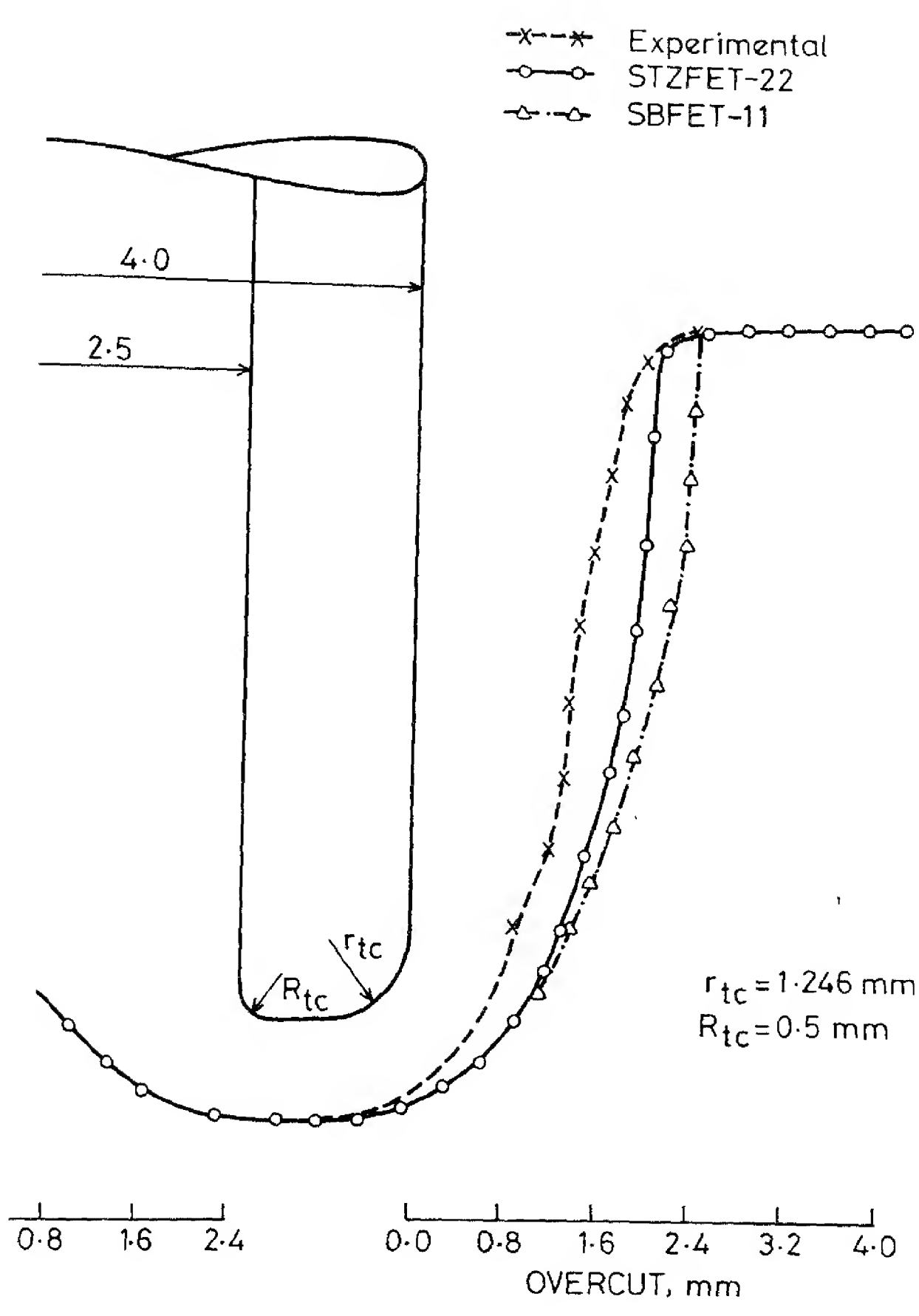
Experimental
STZFET-22
SBFET-11
4·0
2·5
r_{tc}
R_{tc}
r_{tc} = 1·246 mm
R_{tc} = 0·5 mm
0·8
1·6
2·4
0·0
0·8
1·6
2·4
3·2
4·0
OVERCUT, mm

(a)

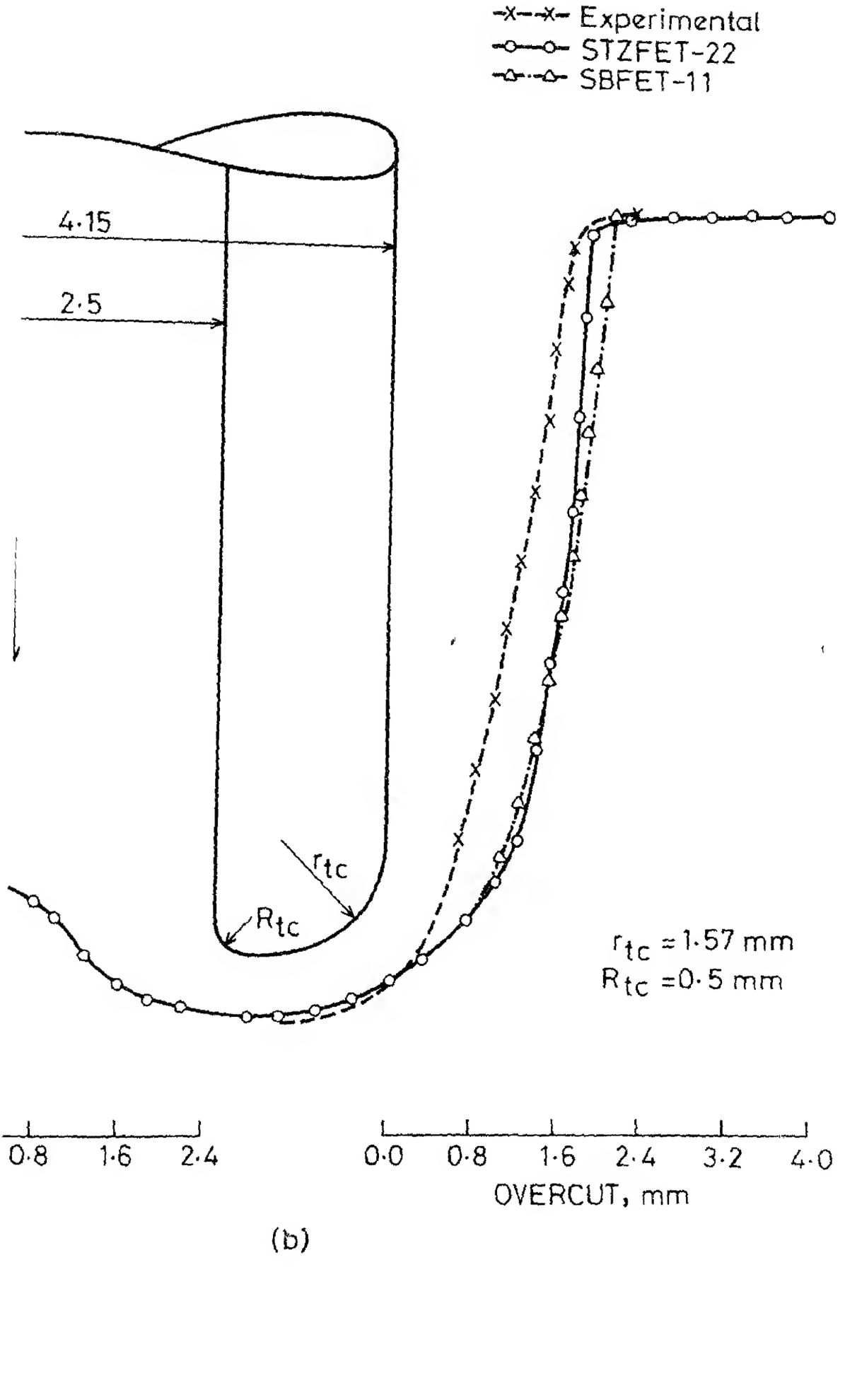
Experimental
STZFET-22
SBFET-11
4·15
2·5
r_{tc}
R_{tc}
r_{tc} = 1·57 mm
R_{tc} = 0·5 mm
0·8
1·6
2·4
0·0
0·8
1·6
2·4
3·2
4·0
OVERCUT, mm

(b)

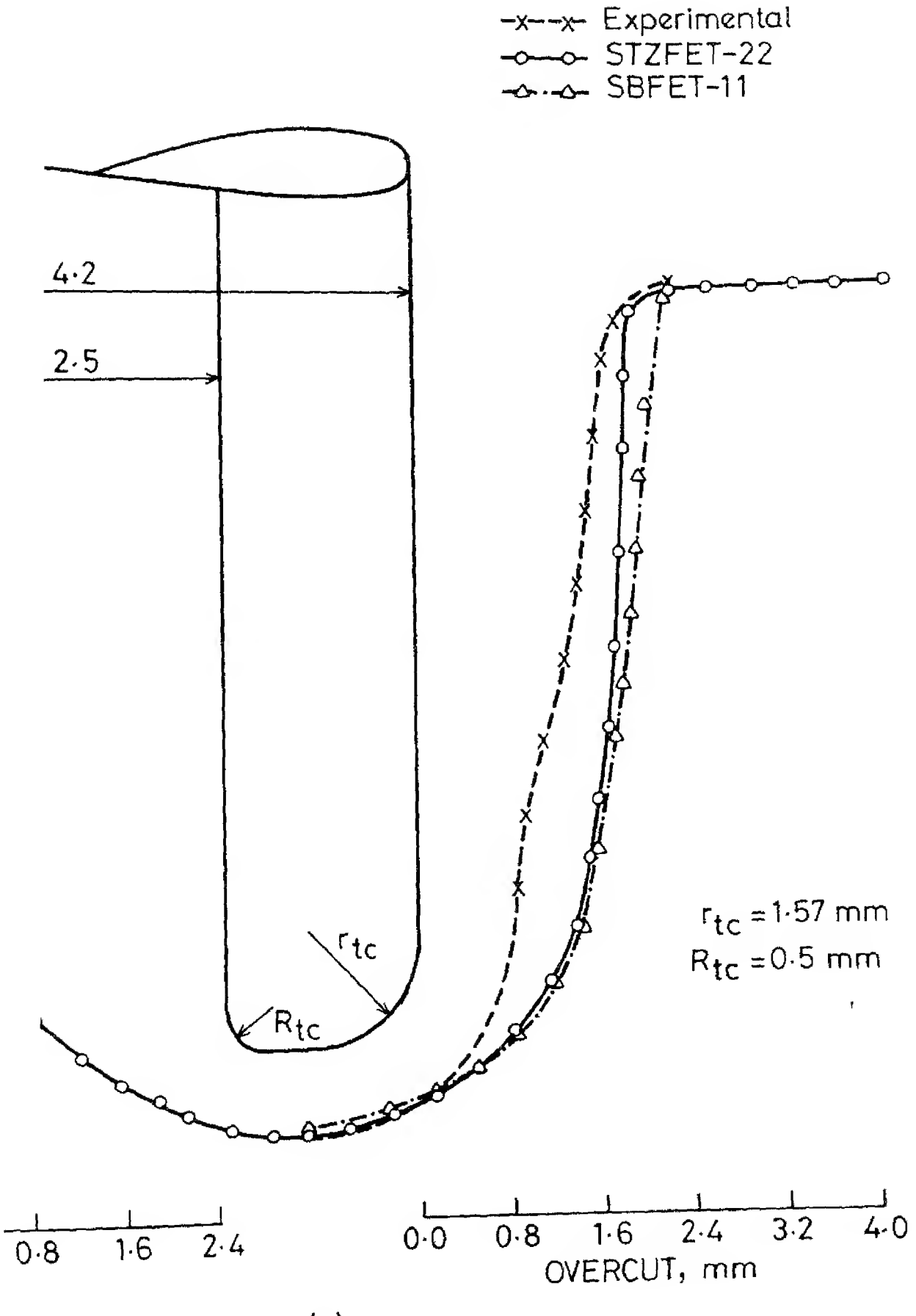
Experimental
STZFET-22
SBFET-11
4·2
2·5
r_{tc}
R_{tc}
r_{tc} = 1·57 mm
R_{tc} = 0·5 mm
0·8
1·6
2·4
0·0
0·8
1·6
2·4
3·2
4·0
OVERCUT, mm

(c)

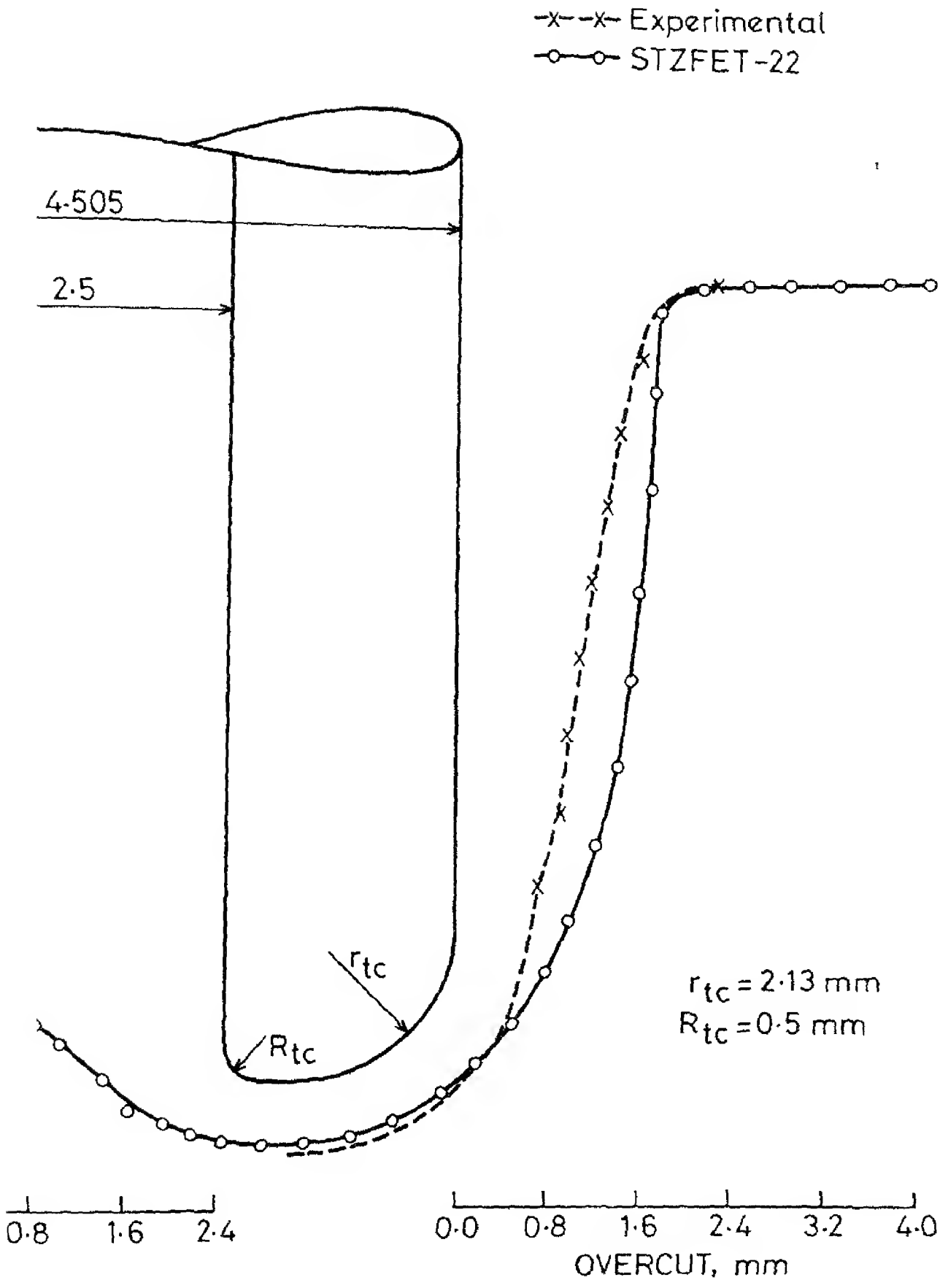

(d)

omparison of experimental and analytical anode profiles btained during ECD

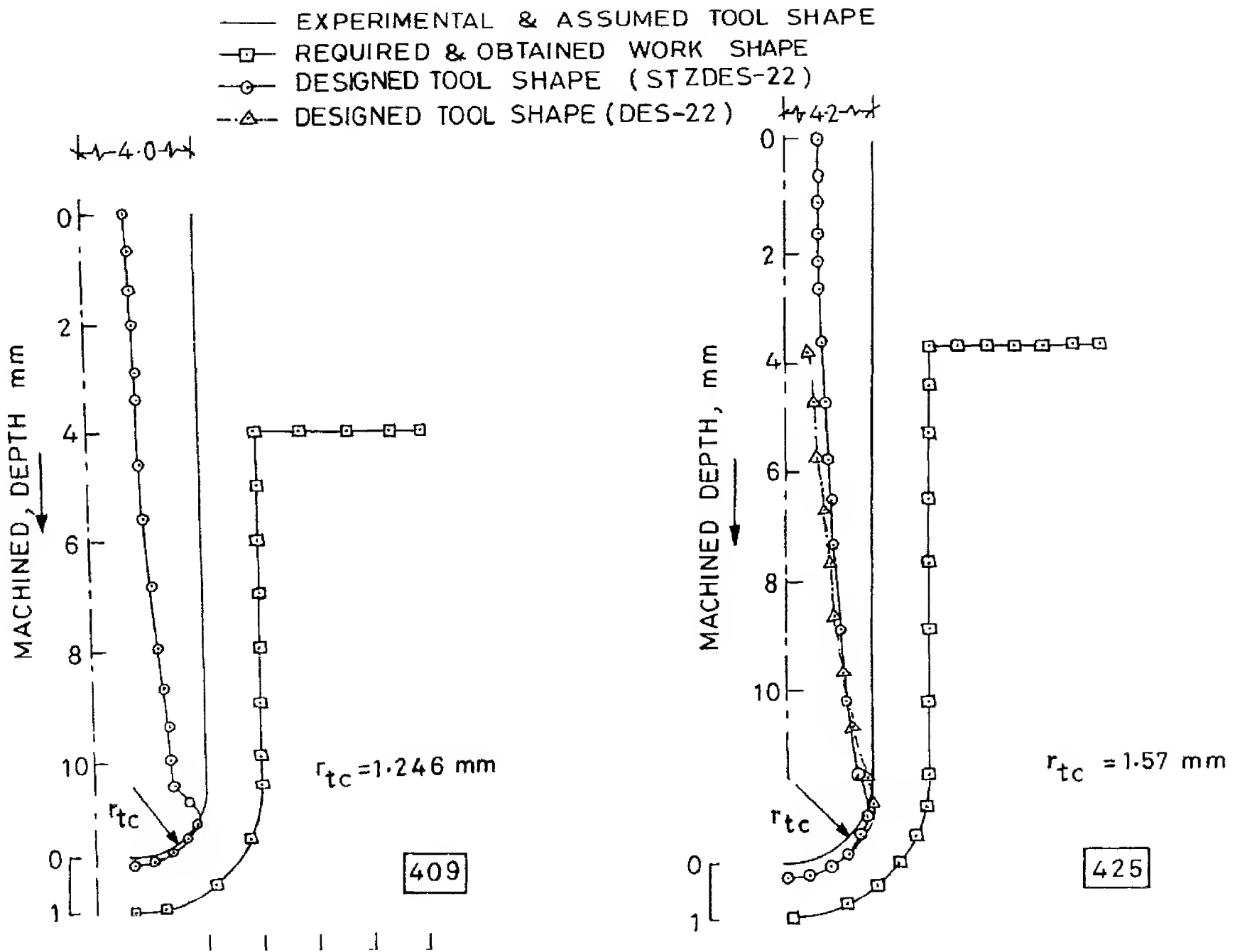
EXPERIMENTAL & ASSUMED TOOL SHAPE
REQUIRED & OBTAINED WORK SHAPE
DESIGNED TOOL SHAPE (STZDES-22)
DESIGNED TOOL SHAPE (DES-22)
4·0
4·2
MACHINED, DEPTH mm
MACHINED DEPTH, mm
0
2
4
6
8
10
1
r_{tc}
r_{tc} =1·246 mm
r_{tc} = 1·57 mm
409
425

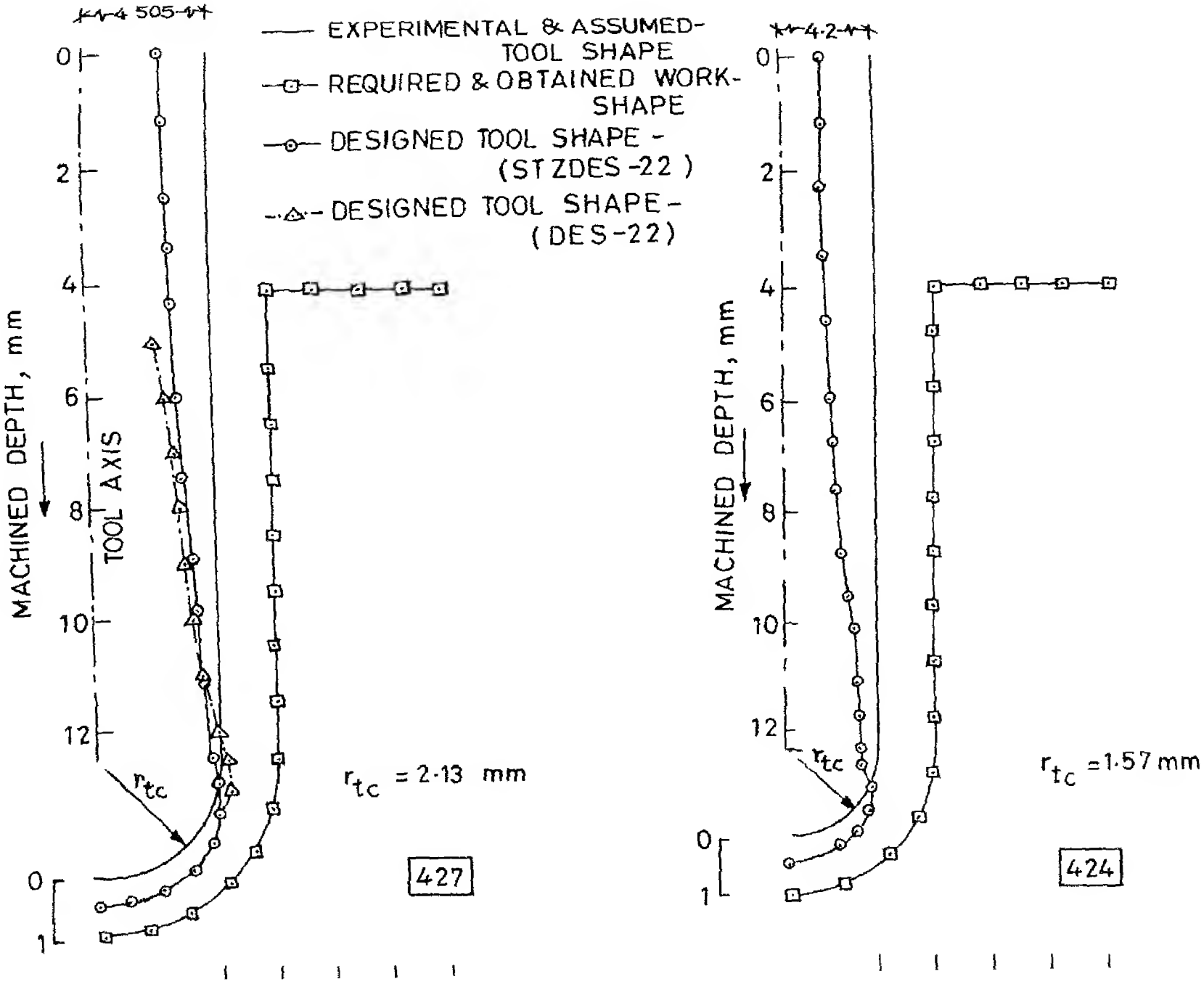
505
EXPERIMENTAL & ASSUMED-TOOL SHAPE
REQUIRED & OBTAINED WORK-SHAPE
DESIGNED TOOL SHAPE - (STZDES-22)
DESIGNED TOOL SHAPE - (DES-22)
MACHINED DEPTH, mm
TOOL AXIS
0
2
4
6
8
10
12
r_{tc}
r_{tc} = 2·13 mm
427
0
1
42
MACHINED DEPTH, mm
0
2
4
6
8
10
12
r_{tc}
r_{tc} = 1·57 mm
424
0
1

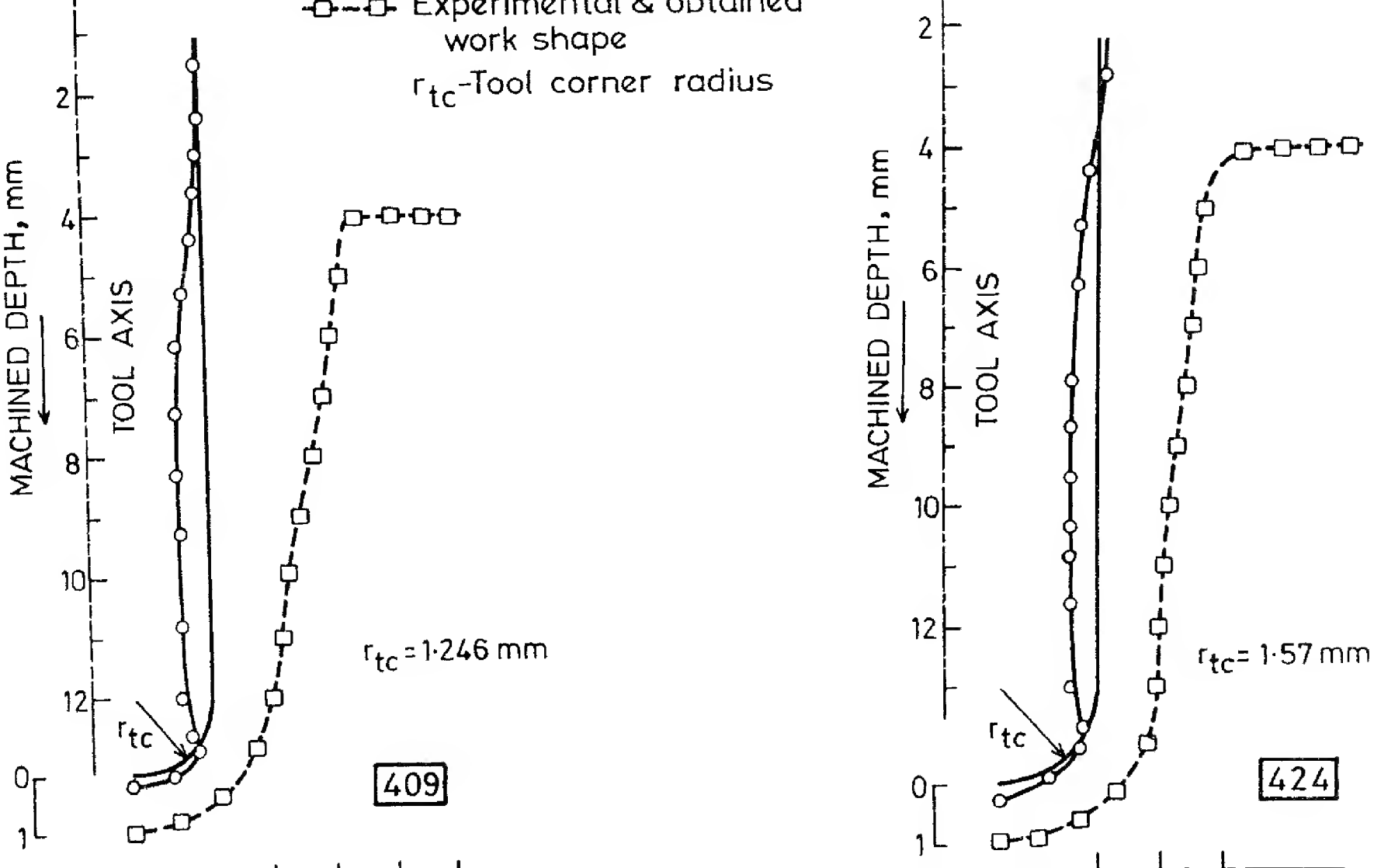
Experimental & obtained work shape
r_{tc}-Tool corner radius
MACHINED DEPTH, mm
TOOL AXIS
r_{tc}
r_{tc} = 1·246 mm
409
r_{tc}= 1·57 mm
424
0
1
2
4
6
8
10
12

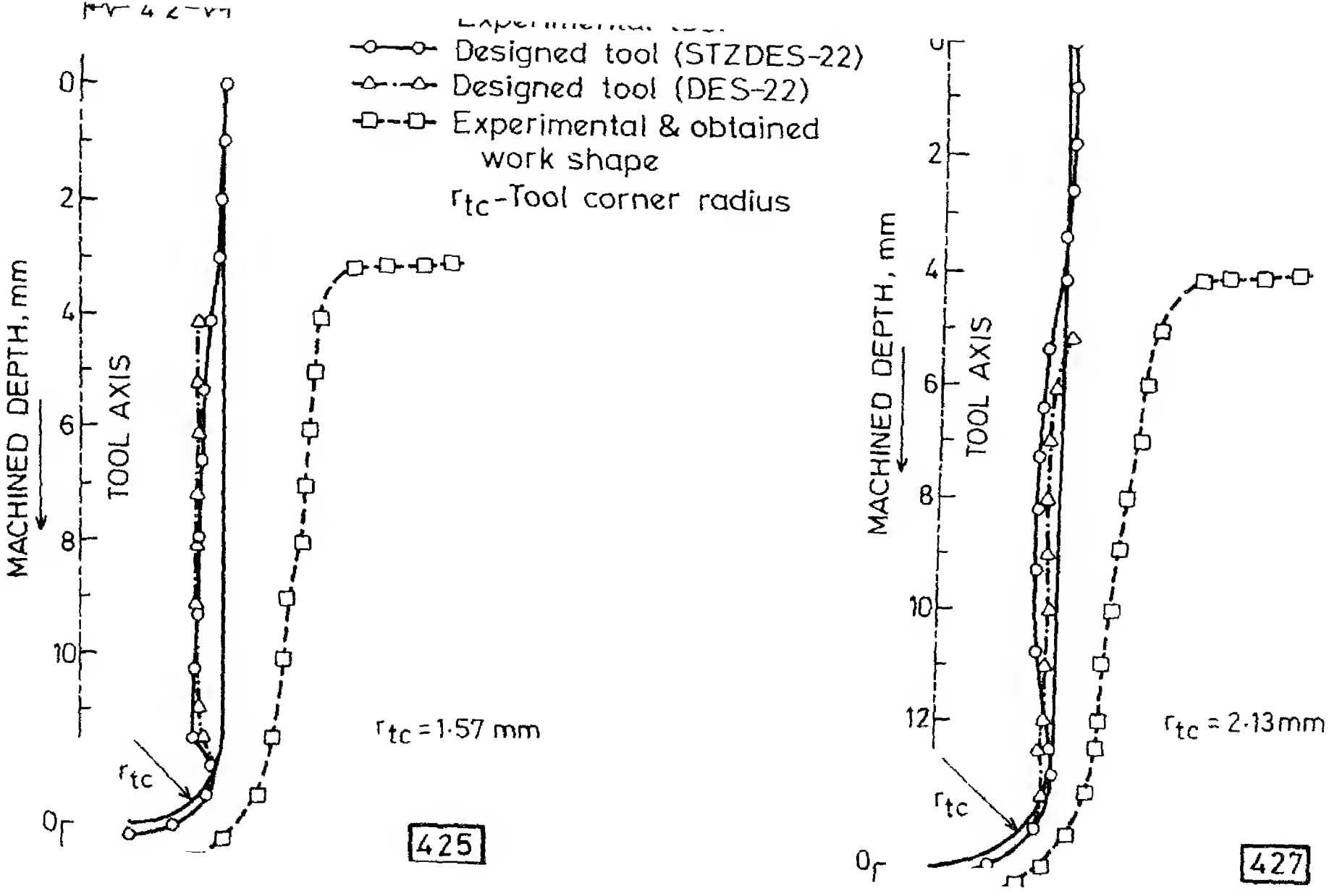
Designed tool (STZDES-22)
Designed tool (DES-22)
Experimental & obtained work shape
r_{tc}-Tool corner radius
MACHINED DEPTH, mm
TOOL AXIS
r_{tc}
r_{tc} = 1·57 mm
425
MACHINED DEPTH, mm
TOOL AXIS
r_{tc}
r_{tc} = 2·13 mm
427

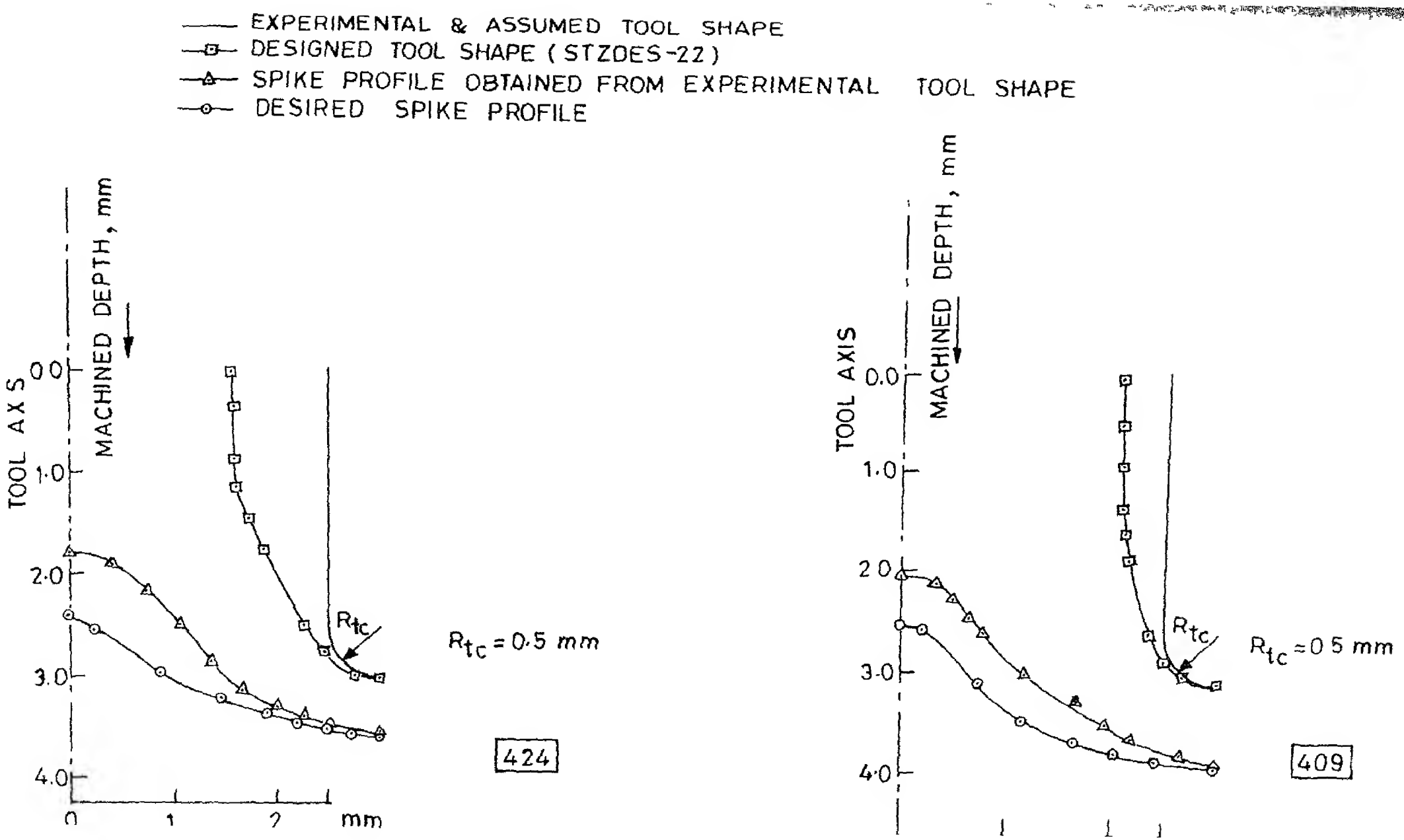
EXPERIMENTAL & ASSUMED TOOL SHAPE
DESIGNED TOOL SHAPE (STZDES-22)
SPIKE PROFILE OBTAINED FROM EXPERIMENTAL TOOL SHAPE
DESIRED SPIKE PROFILE
TOOL AXIS
MACHINED DEPTH, mm
0.0
1.0
2.0
3.0
4.0
0
1
2
mm
Rtc
Rtc = 0.5 mm
424
TOOL AXIS
MACHINED DEPTH, mm
0.0
1.0
2.0
3.0
4.0
Rtc
Rtc = 0.5 mm
409

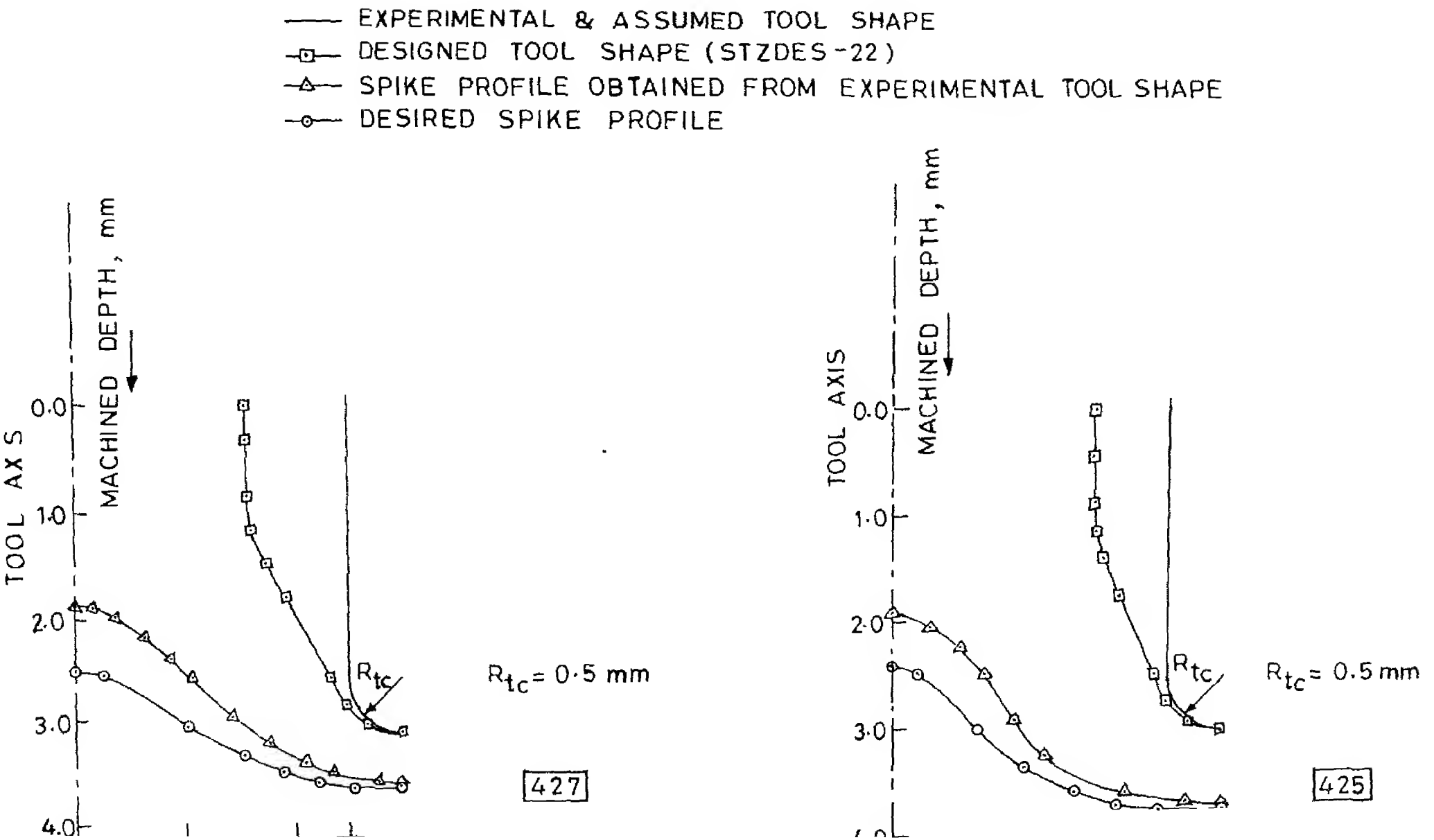
EXPERIMENTAL & ASSUMED TOOL SHAPE
DESIGNED TOOL SHAPE (STZDES-22)
SPIKE PROFILE OBTAINED FROM EXPERIMENTAL TOOL SHAPE
DESIRED SPIKE PROFILE
TOOL AXIS
MACHINED DEPTH, mm
0.0
1.0
2.0
3.0
4.0
R_{tc}
R_{tc} = 0.5 mm
427
TOOL AXIS
MACHINED DEPTH, mm
0.0
1.0
2.0
3.0
R_{tc}
R_{tc} = 0.5 mm
425

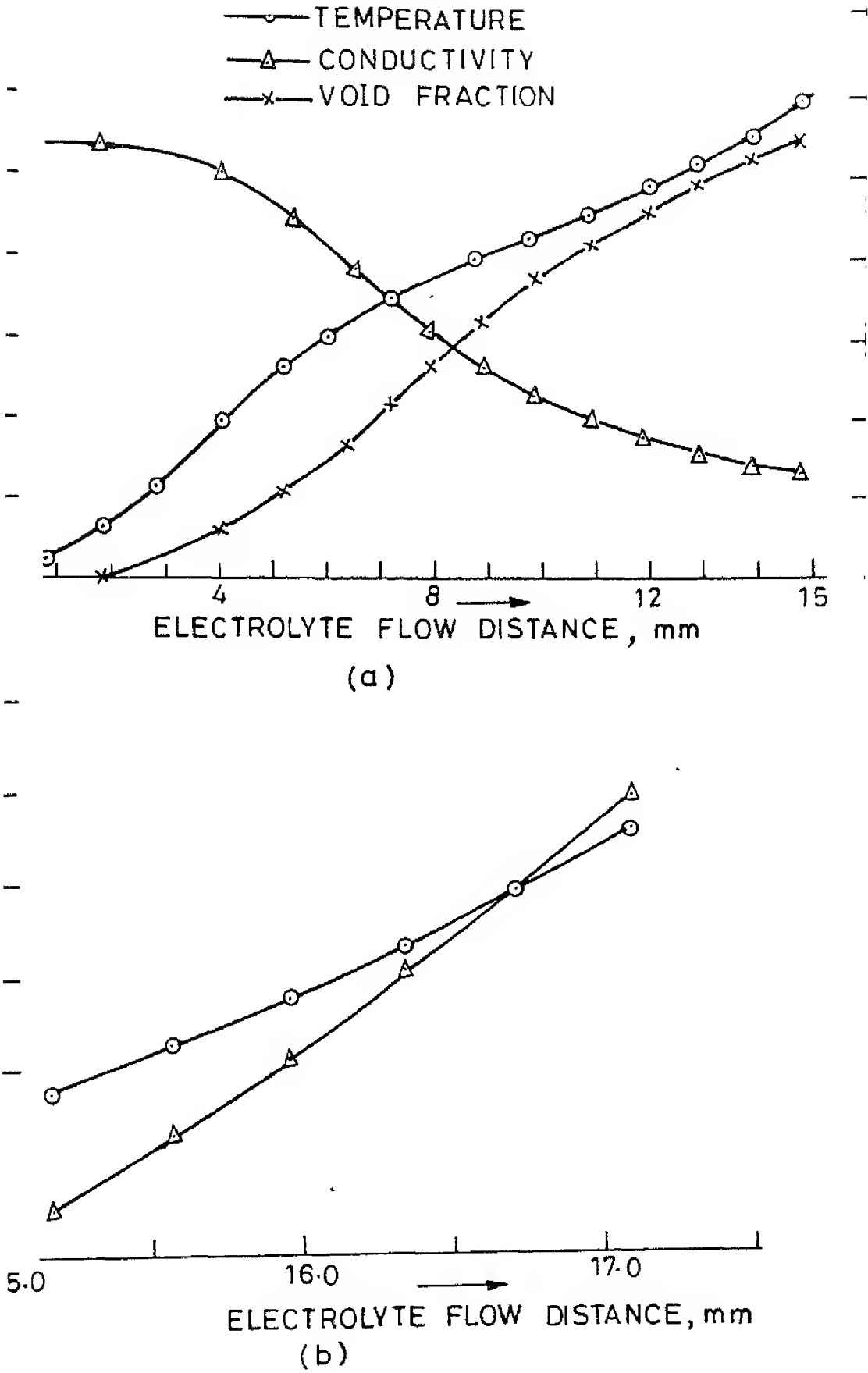

Temperature, Conductivity and Void fraction variation along electrolyte flow path for Job No
a) stagnation, front, transition & side zones
b stray current zone

CHAPTER V

CONCLUSIONS AND SCOPE FOR FUTURE WORK

5.1 CONCLUSIONS

The following conclusions have been drawn from the present work:

- The model STZFET-22 is capable of predicting the nature of variation of current density, temperature, electrolyte conductivity etc. in all the five zones during Electrochemical drilling.
- Designed tool (cathode) shape is not the complementary shape of desired workpiece shape reduced by some machining gap dimensions.
- There is a good agreement between the designed tool and the tool used during experimentation. Thus correction method is capable of designing tools reasonably accurately for Electrochemical drilling.
- The accuracy of correction method depends upon the accuracy of anode shape prediction model. Any discrepancy is anode shape prediction model will be reflected in the designed tool.

5.2 SCOPE FOR FUTURE WORK

The work embodied in this thesis can be extended in the following directions:

(i) An attempt should be made to improve the accuracy of the tool design model by improving the anode shape prediction model in the following ways:

(a) More accurate electrolyte flow velocity distribution should be obtained by solving Navier-Stoke's equations.

(b) In the present analysis, effect of void fraction on conductivity in stagnation zone and stray current zone has been neglected. It would be of interest to know to what degree this assumption caused the predictions to deviate from measured results. So effect of void fraction on conductivity must be analysed.

(ii) Extensive data should be collected about the machining efficiency, electrochemical equivalent of different metals and alloys under different situations, so that accurate prediction of anode profiles can be made.

(iii) Careful experiments should be conducted to find out the spike profile in stagnation zone. The final comparison between the experimental and calculated results must be left to show whether the assumptions made in the analytical model leaves the result sufficiently legitimate for the purpose in hand.

(iv) For better accuracy, models based on two and three dimensional analysis of ECD using isoparametric and higher order elements should be evolved.

(v) For the practical applications (for example, elliptical, parabolic shape drilling, etc.) the tool design models based on three dimensional analysis should be evolved.

(vi) This tool design procedure can be extended to external shaping as well.

REFERENCES

De Barr, A.E. and Oliver, D.A., "Electrochemical Machining", Macdonald and Co. Ltd., 1968.

Acharya, B.G., Jain, V.K. and Batra, J.L., "Multi-objective Optimization of the ECM Process", Precision Engg., Apr. 1986, Vol. 8, No.2, pp.88-95.

Jain, V.K., "Analysis of ECM Process for Anode Shape Prediction", Ph.D. Thesis, University of Roorkee, India, 1980.

Konig, W. and Pahl, D., "Accuracy and Optimal Working Conditions in ECM", Annals CIRP, 1970, Vol. 18, pp. 223-230.

Jain, V.K. and Pandey, P.C., "Tooling Design for ECM", Precision Engg., Vol. 2, No.4, 1980, pp. 195-206.

Tipton, H., "The Determination of Tool Shape for ECM", Machinery and Production Engg., Feb. 1968, pp. 325-328.

Tipton, H., "The Dynamics of ECM", Proc. 5th Int. MTDR Conf., 1964, pp. 509-522.

Ganesh, S. and Rajan, T., "Nomographic Approach for Planning in ECM", J. of Inst. Engrs. (India), Jan. 1979 Vol. 59, pp. 200-204.

Lawrence, P., "Computer Aided Design for ECM Electrodes Int. J. of MTDR, Vol. 21, 1981, pp. 379-385.

Tipton, H., "The Calculation of Tool Shapes for ECM", Fundamentals of ECM (Edited by C.L. Faust), Electrochemical Society (1971), pp. 87-102.

Hopenfeld, J. and Cole, R.R., "ECM - Prediction and Correlation of Process Variables", Trans. ASME, J. of Engg. for Industry, Vol. 88, 1966, pp. 1-7.

Nanayakkara, M.B., et al., "Computation and Verificatic of Workpiece Shape in ECM", 20th Int. MTDR Conf., 1979, pp. 617-624.

Jain, V.K. and Pandey, P.C., "Tooling Design for ECM - A Finite Element Approach", J. of Engg. for Industry, Trans. ASME, May 1981, Vol. 103, pp. 183-190.

Murugan, S., "Prediction of Anode Profile in ECBD and ECBB Operations", M.Tech. Thesis, IIT Kanpur, 1985.

Yogindra, P.G., "Two-Dimensional FE Analysis of Electrochemical Drilling Process for Anode Shape Prediction", M.Tech. Thesis, IIT Kanpur, 1985.

Ravi Raju, K., "Two-Dimensional FE Analysis for Tool Design in ECM", M.Tech. Thesis, IIT Kanpur, 1987.

Narayanan, O.H., Hinduja, S. and Noble, C.F., "The Prediction of Workpiece Shape during ECM by Boundary Element Method", Int. J. of MTDR, Vol. 26, No.3, 1986, pp. 323-338.

Hoar, T.P. and Mears, D.C., "Relationships Between Anodic Passivity, Brightening and Pitting", Corrosion Science, Vol. 5, 1965, pp. 279-286.

Boden, P.J. and Evans, J.M., "Reduction of Stray Current Attack in ECM", Electrochim. Acta, Vol. 16, 1971, pp. 1071-1077.

LaBoda, M.A. and McMillan, M.L., "ECM Tailored for Precision", American Machinist, Dec. 1966, pp. 144-146.

Bannard, J., "A Critical Review of Electrochemical Machining Process", Journal of Applied Electrochemistry Vol. 4, 1974, pp. 229-234.

Larsson, C.N. and Mazaffaruddin, K., "Electrochemical Effects on Shape Reproduction in ECM", 29th Intl. MTDR Conf. Proceedings, 1978, pp. 533-540.

Thorpe, J.F. and Zerkle, R.D., "Analytical Determinatio of Working Gap in ECM", Int. J. of MTDR, Vol. 9, 1969, pp. 131-144.

McGeough, J.A., "Principles of Electrochemical Machinin Chapman and Hall, London (1974).

Reddy, M.S., "Computer Aided Design of Cathode for ECM" M.Tech. Thesis, IIT Kanpur, 1986.

Moir, P.J. and Harvey, S.J., "Electrochemical Machining of Curved Long Flow Path Profiles", Proc. of 16th Int. MTDR Conf., 1976, pp. 283-289.

APPENDIX - I

COMPUTATIONAL DETAILS

This appendix describes the development of generalised computer programs for the computation of anode profiles obtained during ECD using a bare tool (STZFET-22) and for computation of designed tools during ECD (STZDES-22). In these models, three noded triangular elements have been used for discretizing the solution domain. The potential distribution has been obtained by solving the Laplace equation. These programs are capable of automatically generating the global stiffness matrix, applying the prescribed boundary conditions and storing the stiffness matrix in the banded form. The resultant set of equations have been solved by Gauss Elimination Technique. The computational schemes used in anode shape prediction model STZFET-22 and tool design model STZDES-22 are shown in Figures A.1 and A.2 respectively.

BRIEF DESCRIPTION OF SUBROUTINES USED

(I) SUBROUTINE INDATA: This subroutine reads and prints the input data for the problem.

(II) SUBROUTINE XYCORD: It generates the node numbers, X and Y-coordinates for each node, connectivity matrix for the finite element mesh, the various arrays and assigns the boundary conditions for the nodes on the tool and workpiece.

(III) SUBROUTINE BANDW: It determines the band width of the global stiffness matrix.

(IV) SUBROUTINE STIMAT: This subroutine generates the coefficients of elemental stiffness matrices and stores the assembled global stiffness matrix in banded form.

(V) SUBROUTINE ABCOND: This subroutine applies prescribed boundary conditions for the nodes on the tool and the workpiece.

(VI) SUBROUTINE BANSOL: This solves the set of linear simultaneous equations by Gauss elimination method and gives the potential distribution.

(VII) SUBROUTINE VELSTI: This subroutine generates the elemental stiffness matrices and assemble them is global stiffness matrix. It also generates the velocity boundary matrix.

(VIII) SUBROUTINE ABCVEL: This subroutine applies the velocity boundary conditions.

(IX) SUBROUTINE VELSOL: This subroutine solves the set of linear simultaneous equations by Gauss's elimination method.

(X) SUBROUTINE VELCAL: This subroutine calculates the velocities at various nodes on the workpiece.

(XI) SUBROUTINE TEMCON: This subroutine calculates the temperature and current density at various nodes on the workpiece.

(XII) SUBROUTINE CONMOD: This subroutine calculates the electrolyte pressure and void fraction within the IEG. It also modifies the electrolyte conductivity by taking into consideration the void fraction.

(XIII) SUBROUTINE FEDRAT: This subroutine determines the feed rate at various nodes on the workpiece.

(XIV) SUBROUTINE MRR: This subroutine calculates the MRR and IEG at different nodes on the workpiece.

(XV) SUBROUTINE MODY: This subroutine generates new elements at the end of each computational cycle and calculates the Y-coordinates of each node.

(XVI) SUBROUTINE MODX: This subroutine generates the X-coordinates of each node at the end of each computational cycle.

(XVII) SUBROUTINE PRTOUT: This subroutine prints out the required results in a specific format.

(XVIII) SUBROUTINE INITIL: This subroutine initializes the global stiffness matrices and the potential distribution matrices in each cycle of computation.

(XIX) SUBROUTINE DESIGN: This subroutine calculates the error and correction and develops the new tool shape.

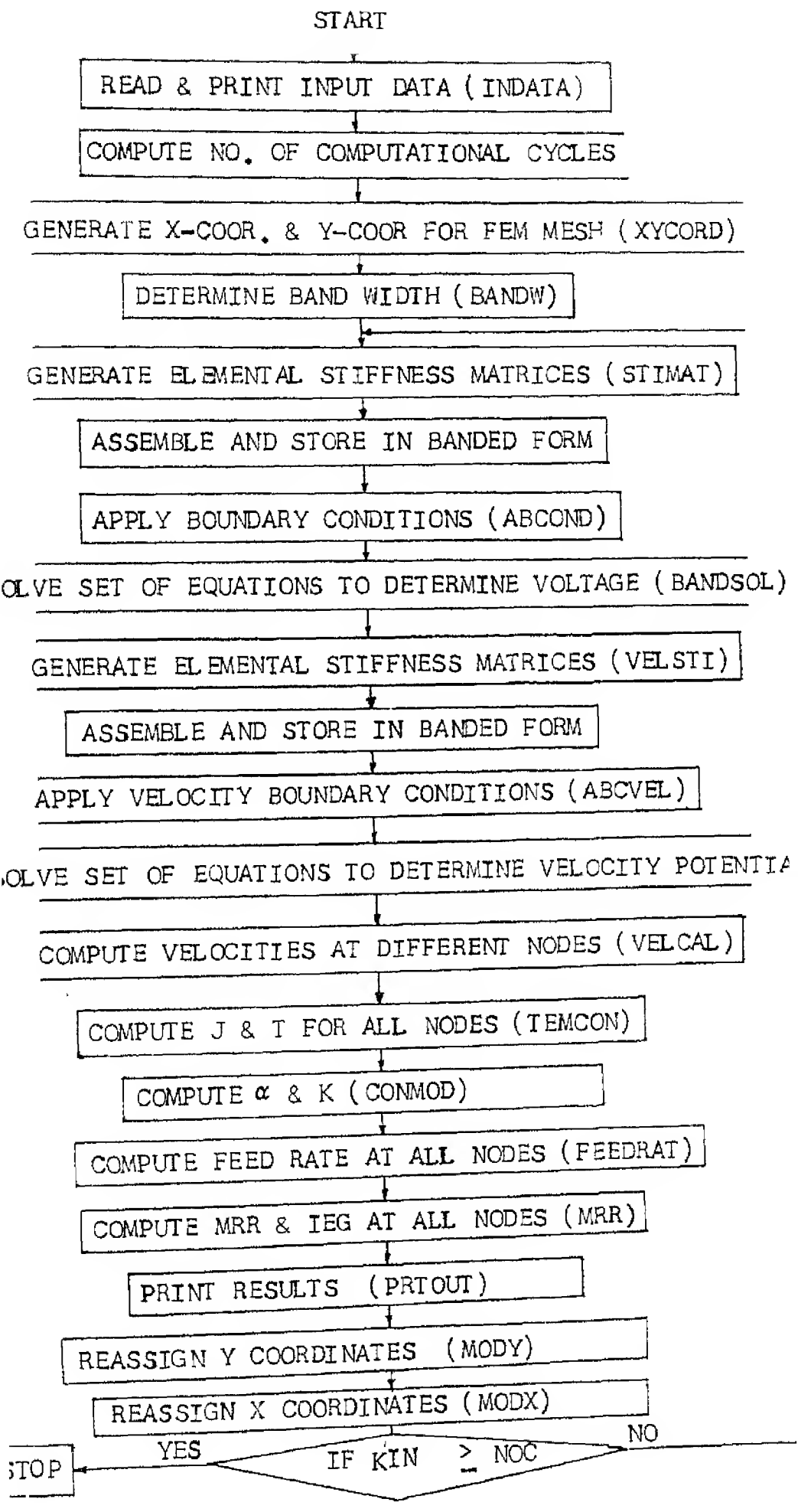
START
READ & PRINT INPUT DATA (INDATA)
COMPUTE NO. OF COMPUTATIONAL CYCLES
GENERATE X-COOR. & Y-COOR FOR FEM MESH (XYCORD)
DETERMINE BAND WIDTH (BANDW)
GENERATE ELEMENTAL STIFFNESS MATRICES (STIMAT)
ASSEMBLE AND STORE IN BANDED FORM
APPLY BOUNDARY CONDITIONS (ABCOND)
OLVE SET OF EQUATIONS TO DETERMINE VOLTAGE (BANDSOL)
GENERATE ELEMENTAL STIFFNESS MATRICES (VELSTI)
ASSEMBLE AND STORE IN BANDED FORM
APPLY VELOCITY BOUNDARY CONDITIONS (ABCVEL)
OLVE SET OF EQUATIONS TO DETERMINE VELOCITY POTENTIA
COMPUTE VELOCITIES AT DIFFERENT NODES (VELCAL)
COMPUTE J & T FOR ALL NODES (TEMCON)
COMPUTE α & K (CONMOD)
COMPUTE FEED RATE AT ALL NODES (FEEDRAT)
COMPUTE MRR & IEG AT ALL NODES (MRR)
PRINT RESULTS (PRTOUT)
REASSIGN Y COORDINATES (MODY)
REASSIGN X COORDINATES (MODX)
IF KIN ≥ NOC
YES
NO
STOP

(a)

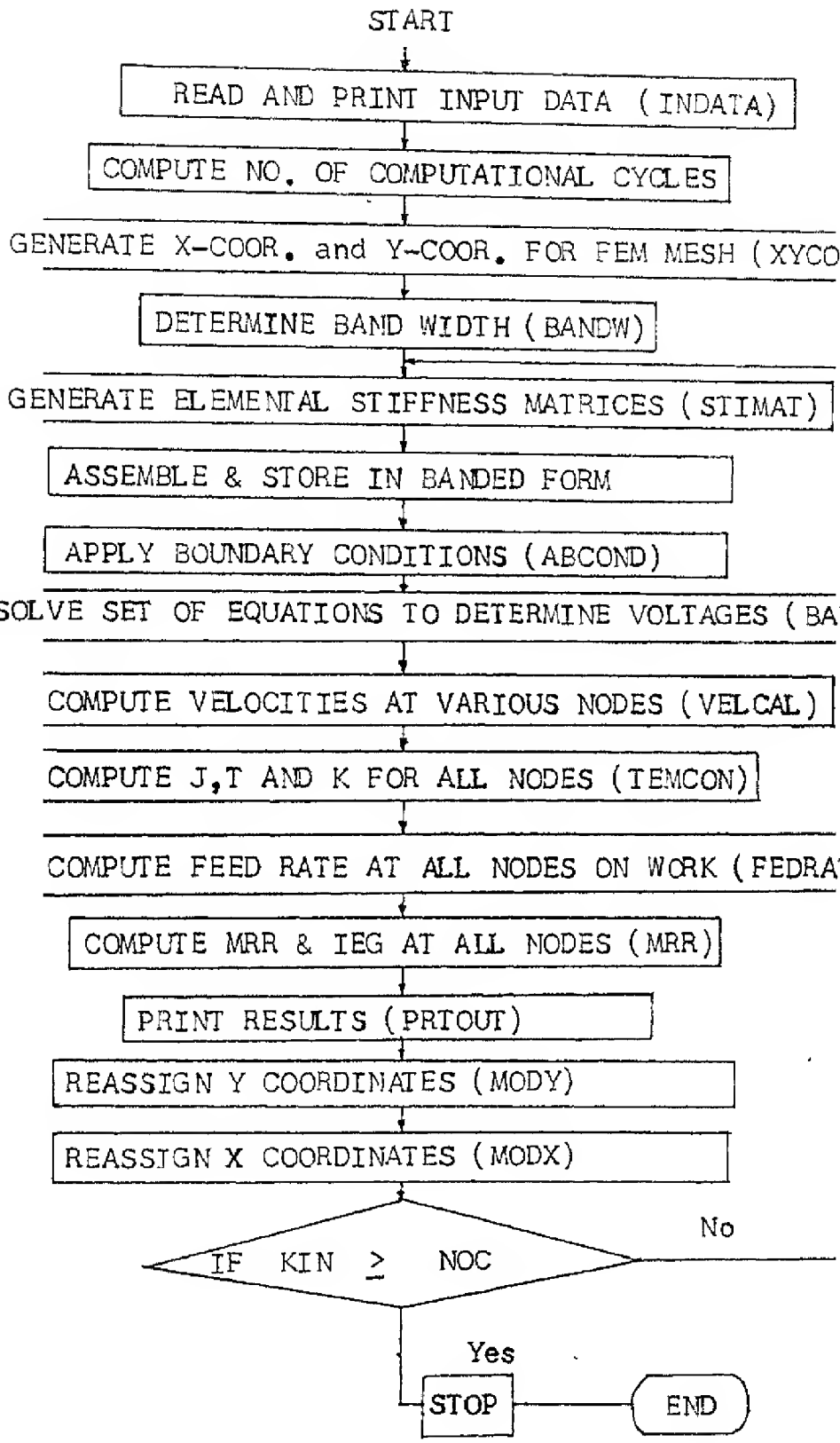

(b)

E A.1 FLOW CHART FOR MODEL STZFET-22

(a) FOR FRONT, TRANSITION, SIDE & STRAY CURI ANALYSIS

(b) FOR STAGNATION ZONE ANALYSIS

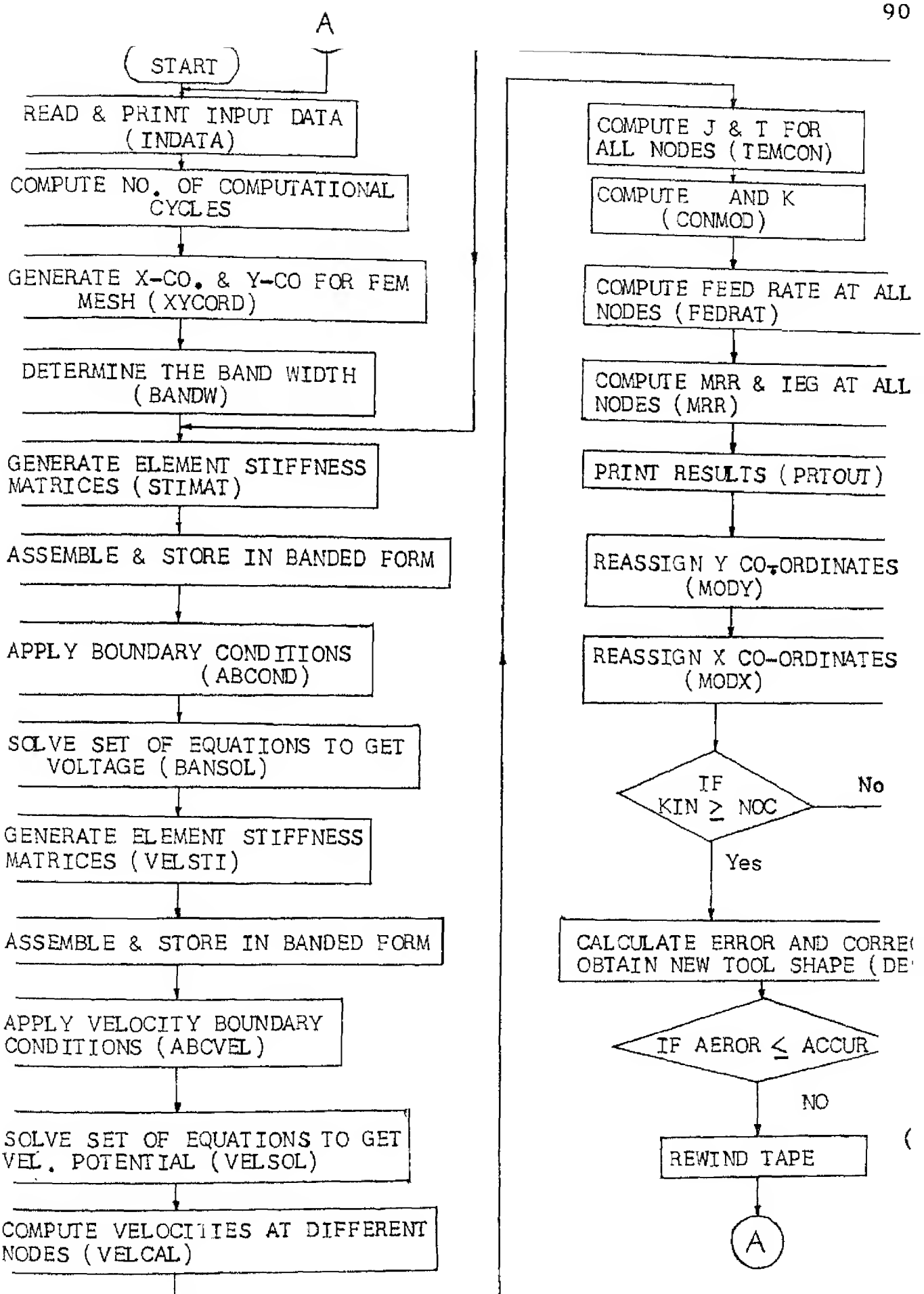
A
START
READ & PRINT INPUT DATA (INDATA)
COMPUTE NO. OF COMPUTATIONAL CYCLES
GENERATE X-CO. & Y-CO FOR FEM MESH (XYCORD)
DETERMINE THE BAND WIDTH (BANDW)
GENERATE ELEMENT STIFFNESS MATRICES (STIMAT)
ASSEMBLE & STORE IN BANDED FORM
APPLY BOUNDARY CONDITIONS (ABCOND)
SOLVE SET OF EQUATIONS TO GET VOLTAGE (BANSOL)
GENERATE ELEMENT STIFFNESS MATRICES (VELSTI)
ASSEMBLE & STORE IN BANDED FORM
APPLY VELOCITY BOUNDARY CONDITIONS (ABCVEL)
SOLVE SET OF EQUATIONS TO GET VEL. POTENTIAL (VELSOL)
COMPUTE VELOCITIES AT DIFFERENT NODES (VELCAL)
COMPUTE J & T FOR ALL NODES (TEMCON)
COMPUTE AND K (CONMOD)
COMPUTE FEED RATE AT ALL NODES (FEDRAT)
COMPUTE MRR & IEG AT ALL NODES (MRR)
PRINT RESULTS (PRTOUT)
REASSIGN Y CO-ORDINATES (MODY)
REASSIGN X CO-ORDINATES (MODX)
IF KIN ≥ NOC
No
Yes
CALCULATE ERROR AND CORRE
OBTAIN NEW TOOL SHAPE (DE
IF AEROR ≤ ACCUR
NO
REWIND TAPE
A

(a

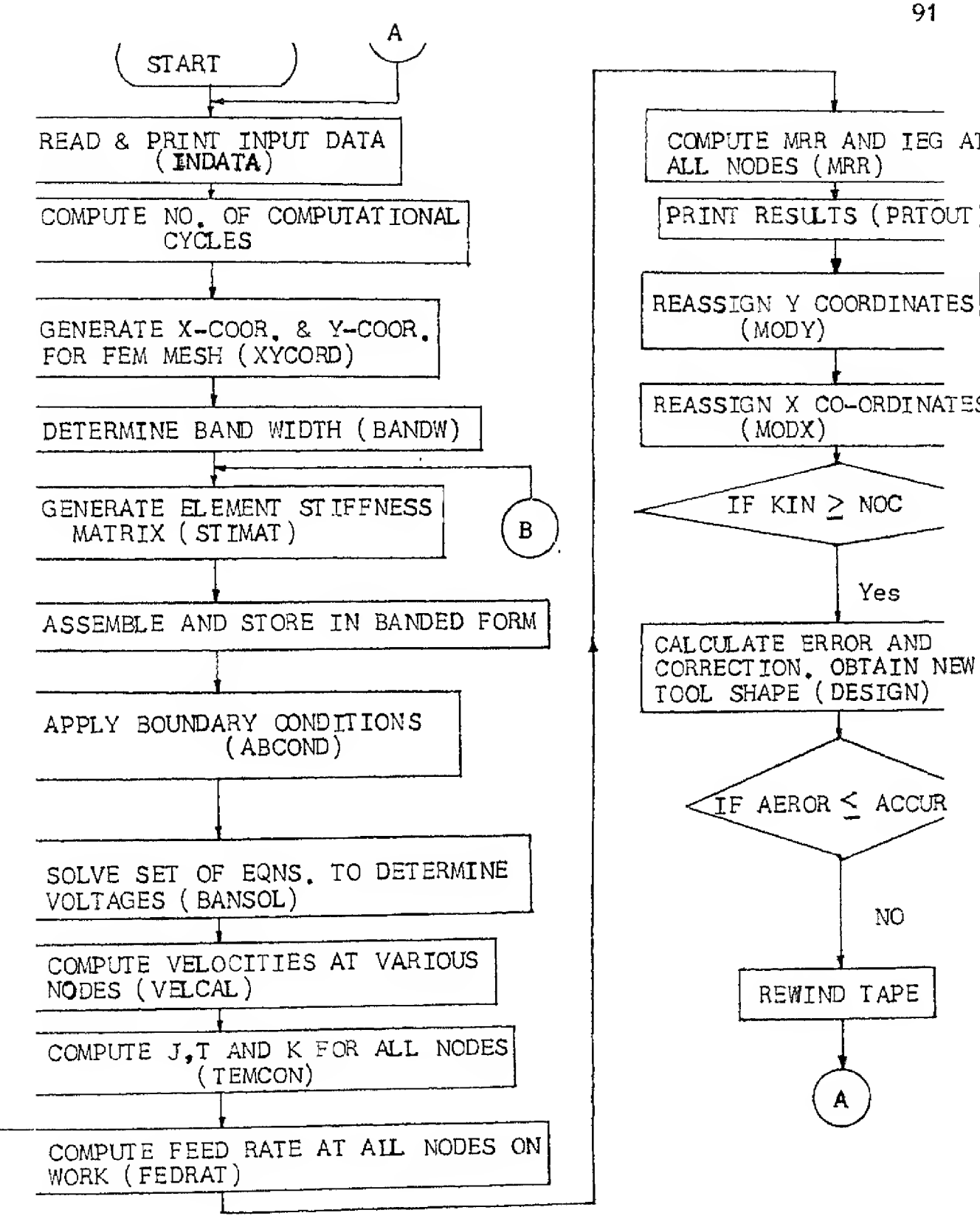

(b)

FIGURE A.2 : FLOW CHART FOR MODEL STZDES 22

(a) FOR FRONT, TRANSITION, SIDE & STRAY CURRENT ZONE ANALYSIS

(b) FOR STAGNATION ZONE ANALYSIS

APPENDIX II

TABLE 1

Identification Number and Hardness of Work Materials [3]

Work Material	Identification number	Average hardness (BHN)
Low alloy steel castings	200-299	239
Low alloy steel castings	400-499	187
Low alloy steel forgings	600-699	218
Low alloy steel forgings	700-799	220

Work Material Composition

Alloying element	Low alloy steel castings	
	200-299	400-499
C	0.094	0.234
S	0.018	0.011
P	0.020	0.014
Si	0.317	0.500
Mn	0.400	1.440
Ni	-	0.095
Cr	0.760	0.260
Mo	0.920	0.073
Cu	-	0.065
Al	-	0.055
Va	Very small	-
Other impurities	-	5 to 6

TABLE 2

Experimental Conditions used during ECM tests [3]

Work material	M.S. low alloy steel casting and low alloy steel forgings
Tool material	Brass
Tool diameter	7 mm to 18 mm
Mode of electrolyte supply	Radial outward flow
Applied voltage	10-60 V
Electrolyte flow rate	6.7×10^{-5} to 15×10^{-5} m^3/sec
Electrolyte conductivity	0.003 to 0.011 Ohm^{-1} mm^{-1}
Machining time	600 to 3600 sec.

TABLE 3

Experimental Conditions used during ECD of Cast Low Alloy Steel [3]

$f = 0.000571$ mm/s; $\dot{Y}_i = 1.0$ mm

Workpiece No.	K_i (Ohm^{-1} mm^{-1})	$\bar{E}_v$ (volt)	$\bar{I}_c$ (ampere)	%
Tool-1	$r_2 = 4.0$	$r_{tc}=1.246$		
413	0.00725	17.75	13.10	90.15
408	0.00725	15.31	16.24	91.70
409	0.00725	21.84	14.14	95.00
406	0.00725	12.94	13.28	86.90
Tool-3	$r_2 = 4.15$	$r_{tc}=1.57$		
407	0.0063	12.93	15.00	93.15
421	0.0070	14.89	16.40	96.20
424	0.0060	18.50	19.86	92.00
425	0.0066	20.49	18.80	91.86
Tool-4	$r_2 = 4.505$	$r_{tc}=2.13$		
429	0.0060	11.57	18.53	94.00
401	0.00547	12.975	22.15	91.82
418	0.00532	15.95	18.40	92.50
427	0.00532	17.62	-	-
402	0.00600	15.87	18.40	93.70

TABLE 4

Voltage Variation during Electro-chemical Drilling (bare type of tool) [3]

Time in min. \ Job No.	421	425	407	409	424	408	427
0	20.5	21.25	19.5	20.75	21.0	16.0	24.0
1	20.0	21.0	18.5	20.25	20.5	15.5	23.0
2	19.0	20.75	17.5	20.0	19.0	18.0	22.0
3	18.0	20.25	17.0	20.0	18.0	17.5	21.0
4	18.0	20.0	15.5	19.8	18.25	17.5	20.5
5	16.5	20.0	14.5	19.75	17.75	16.5	19.0
6	15.5	19.8	14.5	19.8	18.0	16.5	18.75
7	15.5	19.75	14.0	19.8	18.25	16.5	18.5
8	15.0	19.8	14.0	19.6	18.5	16.25	18.5
9	15.0	19.8	13.75	19.25	18.25	16.0	17.0
10	15.0	19.6	13.0	19.0	18.0	15.75	17.0
11	14.5	19.25	12.5	19.0	18.0	15.40	16.5
12	14.0	19.0	12.5	19.0	17.75	15.0	16.5
13	14.5	19.0	12.0	18.8	17.5	15.0	16.5
14	14.5	19.0	11.75	18.5	17.5	15.0	16.5
15	14.5	18.8	12.0	18.5	17.5	14.75	16.625
16	14.0	18.5	11.5	18.5	17.0	14.75	16.5
17	14.0	18.5	11.5	18.5	16.875	15.0	16.5
18	13.5	18.5	11.0	18.25	15.875	15.5	16.5
19	13.5	18.5	11.0	18.5	16.5	15.5	16.5
20	13.5	18.5	11.0	18.5	16.5	16.0	16.5
21	13.5	18.5	11.0	18.5	16.0	17.0	16.5
22	13.5	18.5	10.75	18.5	16.5	17.0	16.5
23	13.5	18.5	10.75	18.5	15.5	16.0	16.5
24	13.5	18.5	11.25	18.5	15.5	16.0	16.5
25	13.25	18.5	11.0	18.25	15.5	13.0	16.0
26	13.0	18.5	11.0	18.25	15.5	13.0	16.0
27	13.5	18.5	11.0	18.25	15.5	13.0	15.75
28	13.25	18.25	11.0	18.0	15.5	13.0	15.75
29	13.0	18.25	11.0	18.0	15.5	13.0	15.5
30	13.0	18.0	11.0	18.0	15.5	13.0	15.5

TABLE 5

Experimental Observations about Overcut in Side Zone during ECD [3]

Job No.	425	427	421	409	408	406
Depth X, mm	Overcut, mm.					
0.0	2.26	2.32	1.71	2.45	2.634	1.902
0.5	1.76	1.73	1.54	2.01	2.46	1.52
1.0	1.695	1.65	1.56	1.84	2.214	1.75
1.5	1.61	1.63	1.4	1.7	2.14	1.33
2.0	1.6	1.44	1.45	1.67	2.02	1.36
2.5	1.51	1.51	1.31	1.57	1.964	1.21
3.0	1.52	1.34	1.36	1.52	1.85	1.25
3.5	-	1.42	1.13	-	1.76	1.11
4.0	1.43	1.12	1.25	1.42	1.67	1.154
4.5	1.33	1.31	1.02	1.38	1.57	1.03
5.0	1.34	1.02	-	1.34	1.48	1.05
5.5	1.23	1.18	0.91	-	1.34	0.924
6.0	1.11	0.91	0.92	1.26	1.28	0.96
6.5	1.1	1.03	0.71	1.26	1.17	0.84
7.0	0.91	0.61	0.715	1.16	1.134	0.87
7.5	0.84	0.61	-	1.11	0.95	0.74
8.0	-	-	0.60	0.82	0.78	0.80